

Reconfigurable Intelligent Surfaces Relying on Non-Diagonal Phase Shift Matrices

Qingchao Li, Mohammed El-Hajjar, *Senior Member, IEEE*, Ibrahim Hemadeh, *Member, IEEE*, Arman Shojaeifard, *Senior Member, IEEE*, Alain A. M. Mourad, Bruno Clerckx, *Senior Member, IEEE*, Lajos Hanzo, *Fellow, IEEE*

Abstract—Reconfigurable intelligent surfaces (RIS) have been actively researched as a potential technique for future wireless communications, which intelligently ameliorate the signal propagation environment. In the conventional design, each RIS element configures and reflects its received signal independently of all other RIS elements, which results in a diagonal phase shift matrix. By contrast, we propose a novel RIS architecture, where the incident signal impinging on one element can be reflected from another element after an appropriate phase shift adjustment, which increases the flexibility in the design of RIS phase shifts, hence, potentially improving the system performance. The resultant RIS phase shift matrix also has off-diagonal elements, as opposed to the pure diagonal structure of the conventional design. Compared to the state-of-art fully-connected/group-connected RIS structures, our proposed RIS architecture has lower complexity, while attaining a higher channel gain than the group-connected RIS structure, and approaching that of the fully-connected RIS structure. We formulate and solve the problem of maximizing the achievable rate of our proposed RIS architecture by jointly optimizing the transmit beamforming and the non-diagonal phase shift matrix based on alternating optimization and semi-definite relaxation (SDR) methods. Moreover, the closed-form expressions of the channel gain, the outage probability and bit error ratio (BER) are derived. Simulation results demonstrate that our proposed RIS architecture results in an improved performance in terms of the achievable rate compared to the conventional architecture, both in single-user as well as in multi-user scenarios.

Index Terms—Reconfigurable intelligent surfaces (RIS), channel gain, outage probability, average bit error ratio (BER), joint beamforming.

I. INTRODUCTION

IN future wireless networks an ultra-high data rate, ultra-low latency, ultra-high reliability and ubiquitous connectivity is required for communication, computation, sensing and location awareness, especially in the Internet of Things

L. Hanzo would like to acknowledge the financial support of the Engineering and Physical Sciences Research Council projects EP/P034284/1 and EP/P003990/1 (COALESCE) as well as of the European Research Council's Advanced Fellow Grant QuantCom (Grant No. 789028). The support of Interdigital is also gratefully acknowledged. (*Corresponding author: Lajos Hanzo.*)

Qingchao Li, Mohammed El-Hajjar and Lajos Hanzo are with the Electronics and Computer Science, University of Southampton, Southampton SO17 1BJ, U.K. (e-mail: Qingchao.Li@soton.ac.uk; meh@ecs.soton.ac.uk; lh@ecs.soton.ac.uk).

Ibrahim Hemadeh, Arman Shojaeifard and Alain A. M. Mourad are with InterDigital, London EC2A 3QR, U.K. (e-mail: Ibrahim.Hemadeh@InterDigital.com; arman.shojaeifard@interdigital.com; Alain.Mourad@interdigital.com).

Bruno Clerckx is with the Communications and Signal Processing Group, Department of Electrical and Electronic Engineering, Imperial College London, London SW7 2AZ, U.K. (email: b.clerckx@imperial.ac.uk).

(IoT) [1], [2]. Hence Boccardi *et al.* [3] identified a range of sophisticated enabling techniques, including massive multiple-input-multiple-output (MIMO) solutions and millimeter wave communications. As an additional promising component, reconfigurable intelligent surfaces (RIS) have also been proposed for future wireless systems to intelligently reconfigure the propagation environment [4]–[11]. Explicitly, in RIS, a large number of passive scattering elements are employed for creating additional signal propagation paths between the base station (BS) and the mobile terminal users, which can substantially enhance the performance, especially when the direct link between the BS and the users is blocked.

Previous contributions on RIS are mainly focused on maximizing the spectral efficiency/achievable rate or minimizing the transmission power [12]–[21]. In [12], Wu and Zhang minimized the transmission power in the downlink of RIS-aided multi-user MIMO systems, where the popular alternating optimization and semi-definite relaxation (SDR) methods were employed for jointly optimizing the active transmission beamforming (TBF) of the BS and the passive beamforming, represented by the RIS phase shift matrix. This was achieved by approximately configuring the RIS reflecting elements. Ning *et al.* [13] maximized the sum-path-gain of RIS-assisted point-to-point MIMO systems, where the low-complexity alternating direction method of multipliers (ADMM) was employed for configuring the RIS phase shift matrix, while the classic singular value decomposition (SVD) was employed for designing the TBF. In [14], the optimal closed-form solution of the phase shift matrix and TBF were derived by Wang *et al.* for single-user multiple-input-single-output (MISO) millimeter wave systems.

Additionally, in order to reduce the overhead of channel estimation, Han *et al.* [15] maximized the ergodic spectral efficiency of RIS-assisted systems communicating over Rician fading channels, relying on the angle of arrival (AoA) and angle of departure (AoD) information. The problem of maximizing the ergodic spectral efficiency based on statistical CSI in Rician fading channels was studied in [16], where Wang *et al.* considered the effect of channel correlation on the ergodic spectral efficiency.

While considering quantized RIS phase shifts, Wu and Zhang [17] employed the popular branch-and-bound method and an exhaustive search method for single-user and multi-user RIS-assisted systems, respectively. The branch-and-bound algorithm was also employed by Zhang *et al.* [18] to design a discrete phase shift matrix, where the RIS has the dual functions of both reflection and refraction. In [19], the local

methods are formulated in Section III. Our theoretical analysis and simulation results are presented in Section IV and Section V, respectively. Finally, we conclude in Section VI.

Notations: Vectors and matrices are denoted by boldface lower and upper case letters, respectively. $(\cdot)^T$, $(\cdot)^H$ represent the operation of transpose and Hermitian transpose, respectively. $\mathbb{C}^{m \times n}$ denotes the space of $m \times n$ complex-valued matrix. $[\mathbf{a}]_i$ represents the i th element in vector \mathbf{a} , and $[\mathbf{A}]_{i,j}$ represents the (i,j) th element in matrix \mathbf{A} . $\text{diag}\{\mathbf{a}\}$ denotes a diagonal matrix with each element being the elements in vector \mathbf{a} , \mathbf{I} represents the identity matrix. $\text{Tr}(\mathbf{A})$, $\text{Rank}(\mathbf{A})$ and $|\mathbf{A}|$ represent the trace, rank and determinant of matrix \mathbf{A} , respectively. $\mathbf{A} \succeq 0$ indicates that \mathbf{A} is a positive semi-definite matrix. $|a|$ (or $|\mathbf{a}|$) and $\angle a$ (or $\angle \mathbf{a}$) represent the amplitude and phase of the complex scalar a (or complex vector \mathbf{a}), respectively. $\|\mathbf{a}\|$ denotes the 2-norm of vector \mathbf{a} . $f_X(x)$ and $F_X(x)$ are the probability density function (PDF) and cumulative distribution function (CDF) of random variables X . A circularly symmetric complex Gaussian random vector with mean μ and covariance matrix Σ is denoted as $\mathcal{CN}(\mu, \Sigma)$. $\mathbb{E}(X)$ represents the mean of the random variable X .

II. SYSTEM MODEL

A. Channel Model

The RIS-assisted system model is illustrated in Fig. 1, including a BS having M transmit antennas, K single-antenna mobile receivers, and a RIS with N elements. The direct link between the BS and the users is blocked, while the RIS creates additional communication links arriving from the BS to the users. The link spanning from the BS to the RIS is denoted as $\mathbf{G} = [\mathbf{g}_1, \mathbf{g}_2, \dots, \mathbf{g}_M] \in \mathbb{C}^{N \times M}$, where $\mathbf{g}_m \in \mathbb{C}^{N \times 1}$ ($m = 1, 2, \dots, M$) represents the channel vector from the m th BS antenna to the RIS. The links impinging from the RIS to the users are denoted as $\mathbf{H} = [\mathbf{h}_1, \mathbf{h}_2, \dots, \mathbf{h}_K]^H \in \mathbb{C}^{K \times N}$, where $\mathbf{h}_k^H \in \mathbb{C}^{1 \times N}$ ($k = 1, 2, \dots, K$) represents the channel vector from the RIS to the k th single-antenna receiver. We employ the far field RIS channel model, since the size of the RIS is negligible compared to both the BS-RIS distance and to the RIS-user distance [25]. Additionally, we consider a distance-dependent path loss model, and Rician channel model for the small scaling fading [12].

The Rician channel model from the BS to the RIS is given by

$$\mathbf{G} = \sqrt{\frac{\kappa_{\mathbf{G}}}{1 + \kappa_{\mathbf{G}}}} \overline{\mathbf{G}} + \sqrt{\frac{1}{1 + \kappa_{\mathbf{G}}}} \tilde{\mathbf{G}}, \quad (1)$$

where $\kappa_{\mathbf{G}}$ is the Rician factor, $\overline{\mathbf{G}} \in \mathbb{C}^{N \times M}$ and $\tilde{\mathbf{G}} \in \mathbb{C}^{N \times M}$ represent the line-of-sight (LoS) and non-line-of-sight (NLoS) components, respectively.

The LoS component $\overline{\mathbf{G}}$ is expressed as

$$\overline{\mathbf{G}} = \sqrt{\varrho_t} \mathbf{f}_{\text{RIS}}^A(\phi^A, \varphi^A) \mathbf{f}_{\text{BS}}^D(\psi^D), \quad (2)$$

where $\varrho_t = C_0 d_t^{-\alpha_t}$ denotes the path loss of the BS-RIS link, in which d_t denotes the distance between the BS and the RIS. C_0 is the path loss at the reference distance of 1 meter, and α_t is the BS-RIS path loss exponent. $\mathbf{f}_{\text{BS}}^D(\psi^D)$ is the response

of the M -antenna uniform linear array (ULA) at the BS, based on [26]

$$\mathbf{f}_{\text{BS}}^D(\psi^D) = \left[1, e^{-j2\pi \frac{\delta_a}{\lambda} \sin \psi^D}, \dots, e^{-j2\pi \frac{\delta_a}{\lambda} (M-1) \sin \psi^D} \right], \quad (3)$$

where δ_a is the distance between adjacent BS antennas, λ is carrier wavelength, ψ^D is the angle of departure (AoD) of signals from the BS. $\mathbf{f}_{\text{RIS}}^A(\phi^A, \varphi^A)$ is the response of an $N = N_x \times N_y$ uniform rectangular planar array (URPA) at the RIS, given by [26]

$$\mathbf{f}_{\text{RIS}}^A(\phi^A, \varphi^A) = \left[1, \dots, e^{-j2\pi \frac{\delta_0}{\lambda} (n_x \sin \phi^A \cos \varphi^A + n_y \cos \phi^A)}, \dots, e^{-j2\pi \frac{\delta_0}{\lambda} ((N_x-1) \sin \phi^A \cos \varphi^A + (N_y-1) \cos \phi^A)} \right]^T, \quad (4)$$

where $0 \leq n_x \leq N_x - 1$, $0 \leq n_y \leq N_y - 1$, δ_0 is the distance between adjacent RIS elements, ϕ^A and φ^A are the elevation and azimuth angle of arrival (AoA) of signals to the RIS, respectively.

The NLoS component $\tilde{\mathbf{G}} = [\tilde{\mathbf{g}}_1, \tilde{\mathbf{g}}_2, \dots, \tilde{\mathbf{g}}_M]$, $\tilde{\mathbf{g}}_m \in \mathbb{C}^{N \times 1}$ is given by

$$\tilde{\mathbf{g}}_m \sim \mathcal{CN}(\mathbf{0}, \varrho_t \mathbf{I}), \quad m = 1, 2, \dots, M. \quad (5)$$

The Rician channel model from the RIS to the k th user

$$\mathbf{h}_k^H = \sqrt{\frac{\kappa_{\mathbf{h}_k}}{1 + \kappa_{\mathbf{h}_k}}} \overline{\mathbf{h}}_k^H + \sqrt{\frac{1}{1 + \kappa_{\mathbf{h}_k}}} \tilde{\mathbf{h}}_k^H, \quad (6)$$

where $\kappa_{\mathbf{h}_k}$ is the Rician factor, $\overline{\mathbf{h}}_k^H \in \mathbb{C}^{1 \times N}$ and $\tilde{\mathbf{h}}_k^H \in \mathbb{C}^{1 \times N}$ represent the LoS and NLoS components, respectively.

The LoS component $\overline{\mathbf{h}}_k^H$ is expressed as [26]

$$\overline{\mathbf{h}}_k^H = \mathbf{f}_{\text{RIS}}^{D,kH}(\phi^{D,k}, \varphi^{D,k}), \quad (7)$$

where $\mathbf{f}_{\text{RIS}}^{D,kH}(\phi^{D,k}, \varphi^{D,k})$ is the response of N -element URPA at the RIS, given by [26]

$$\begin{aligned} \mathbf{f}_{\text{RIS}}^{D,kH}(\phi^{D,k}, \varphi^{D,k}) &= \sqrt{\varrho_{r,k}} \left[1, \dots, e^{-j2\pi \frac{\delta_0}{\lambda} (n_x \sin \phi^{D,k} \cos \varphi^{D,k} + n_y \cos \phi^{D,k})}, \dots, \right. \\ &\quad \left. e^{-j2\pi \frac{\delta_0}{\lambda} ((N_x-1) \sin \phi^{D,k} \cos \varphi^{D,k} + (N_y-1) \cos \phi^{D,k})} \right], \quad (8) \end{aligned}$$

where $\varrho_{r,k} = C_0 d_{r,k}^{-\alpha_r}$ denotes the path loss from the RIS to the k th user, in which $d_{r,k}$ denotes the distance between the RIS and the k th user, α_r is the RIS-user path loss exponent, and $\phi^{D,k}$ and $\varphi^{D,k}$ are the elevation and azimuth AoD of signals from the RIS to the k th user, respectively.

The NLoS component $\tilde{\mathbf{h}}_k$ is given by

$$\tilde{\mathbf{h}}_k \sim \mathcal{CN}(\mathbf{0}, \varrho_{r,k} \mathbf{I}), \quad k = 1, 2, \dots, K. \quad (9)$$

In this paper, we assume that instantaneous CSI knowledge can be attained at the BS.

In our RIS-assisted system, the signal is precoded by the TBF at the BS and transmitted to the RIS. The RIS configures the phase shifts of the impinging signals and then reflects them to the users. Therefore, the system model is represented as

$$\mathbf{y} = \sqrt{P_t} \mathbf{H} \mathbf{O} \mathbf{G} \mathbf{W} \sqrt{\Lambda} \mathbf{x} + \mathbf{n}, \quad (10)$$

where $\mathbf{x} \in \mathbb{C}^{K \times 1}$ is the transmitted signal vector, $\mathbf{y} \in \mathbb{C}^{K \times 1}$ is the received signal vector, $\mathbf{n} \sim \mathcal{CN}(\mathbf{0}, \sigma_n^2 \mathbf{I}) \in \mathbb{C}^{K \times 1}$ is the circularly symmetric complex Gaussian noise, $\mathbf{W} = [\mathbf{w}_1, \mathbf{w}_2, \dots, \mathbf{w}_K] \in \mathbb{C}^{M \times K}$ represents the active TBF matrix at the BS, P_t is the total transmitted power of the BS, and $\Lambda = \text{diag}\{\lambda_1, \lambda_2, \dots, \lambda_K\}$ is a diagonal power allocation

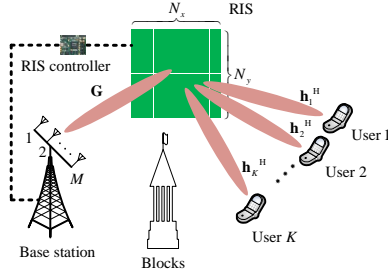


Fig. 1. The employed RIS-assisted wireless communication system model, including a M -antenna base station, K single-antenna users and a RIS with $N = N_x \times N_y$ elements.

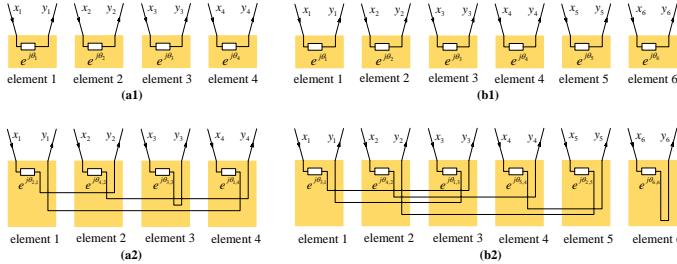


Fig. 2. An example of illustration for the conventional RIS architecture having $N = 4$ elements and $N = 6$ elements in (a1) and (b1) respectively, and the proposed RIS architecture having $N = 4$ elements with the bijection function $\mathcal{M} : \{1, 2, 3, 4\} \rightarrow \{2, 4, 3, 1\}$ and $N = 6$ elements with the bijection function $\mathcal{M} : \{1, 2, 3, 4, 5, 6\} \rightarrow \{3, 4, 1, 5, 2, 6\}$ in (a2) and (b2) respectively.

matrix, where λ_k represents the power allocated to the signal transmitted to the k th user. Hence, in order to normalize the transmit power, we have the following constraints: $\|\mathbf{x}\| = 1$, $\|\mathbf{w}_k\| = 1$, and $\lambda_1 + \lambda_2 + \dots + \lambda_K = 1$. Still referring to (10), Θ represents the RIS phase shift matrix, which is diagonal in the conventional RIS architecture, while it is non-diagonal in our proposed RIS architecture. Our objective is to jointly optimize the RIS phase shift matrix Θ , the TBF matrix \mathbf{W} and the power allocation matrix Λ for maximizing the achievable rate.

In a practical RIS-assisted wireless system as shown in Fig. 1, the phase shift matrix Θ , the TBF matrix \mathbf{W} and the power allocation matrix Λ are jointly optimized at the BS by exploiting the CSI available, i.e. the BS-RIS channel matrix \mathbf{G} and the RIS-users channel matrix \mathbf{H} . Then, using the BS-RIS controller link, the optimized phase shift matrix Θ is transmitted to the RIS controller, which is responsible for reconfiguring the phase applied to the RIS elements.

In the following, we will briefly highlight the conventional RIS architecture, where the phase shift matrix is diagonal. Then, our proposed non-diagonal RIS architecture will be presented.

B. RIS Architecture

1) *Conventional RIS Architecture*: Fig. 2 (a1) shows an example of a conventional 4-element RIS architecture, where each RIS element is ‘single-connected’, i.e. the signal impinging on the i th element is only reflected from the i th element after phase shift adjustment. Similarly, a conventional 6-element RIS architecture is showed in Fig. 2 (b1). In conventional RIS-assisted wireless communication systems, each RIS element changes the phase of the impinging signals independently, that is [5]

$$y_i = \beta_i x_i e^{j\theta_i}, \quad i = 1, 2, \dots, N, \quad (11)$$

where x_i and y_i represent the incident signal and reflected signal of the i th RIS element, respectively. The amplitude gain β_i is set to 1 to realize full reflection, and the phase shift $\theta_i \in [0, 2\pi)$ can be configured for maximizing the channel gain [25]. Since the phase shift of each RIS element is configured independently, the phase shift matrix, denoted as $\bar{\Theta}$ ¹, is diagonal and can be represented as

$$\bar{\Theta} = \text{diag}\{e^{j\theta_1}, e^{j\theta_2}, \dots, e^{j\theta_N}\}. \quad (12)$$

Hence, the equivalent channel spanning from the m th BS transmit antenna to the k th user can be represented as

$$\begin{aligned} \mathbf{h}_k^H \bar{\Theta} \mathbf{g}_m &= \sum_{i=1}^N [\mathbf{h}_k^H]_i e^{j\theta_i} [\mathbf{g}_m]_i \\ &= \sum_{i=1}^N |[\mathbf{h}_k^H]_i| \cdot |[\mathbf{g}_m]_i| \cdot e^{j(\theta_i + \angle[\mathbf{h}_k^H]_i + \angle[\mathbf{g}_m]_i)}, \end{aligned} \quad (13)$$

which includes the BS-RIS channel, the phase shift applied at the RIS and the RIS-user channel.

On the other hand, if there is a connection between the RIS elements, i.e. the incident signal impinging on the i th element can be reflected from other elements, then we will have more flexibility in the design of the RIS phase shift matrix, which can provide an improved performance. The one and only contribution on RIS element cooperation, which was termed as the fully-connected and group-connected RIS architecture, was disseminated by Shen *et al.* [24]. In their solution, the signal impinging on each RIS element was divided into N components, and these N signal components are reflected from N RIS elements after phase shift configuration. This fully connected RIS architecture attains a substantial channel gain. However, its performance enhancement is achieved at the cost of having more entries in the phase shift matrix to optimize, which includes $N \times N$ elements, as opposed to having only N non-zero elements in the conventional design. Furthermore, extra information has to be transmitted over the BS-RIS controller link. On the other hand, the group-connected architecture has significantly lower complexity than the fully-connected architecture, which imposes a modest performance loss. Hence, we propose a novel RIS architecture, which approaches the fully-connected performance at a significantly reduced complexity.

2) *The proposed RIS Architecture*: Explicitly, we design a novel RIS architecture, where the signal impinging on the i th element can be reflected from another one element, denoted as the i' th element, after phase shift adjustment. The relationship between the incident signals and the reflected signals can be represented as

$$y_{i'} = x_i e^{j\theta_{i',i}}, \quad (14)$$

where i belongs to the RIS element index set of incident signals $I : \{1, 2, \dots, N\}$, and i' belongs to the RIS element index set of reflected signals $I' : \{1, 2, \dots, N\}$. There is a bijective function $\mathcal{M} : I \rightarrow I'$, and $i' = \mathcal{M}(i)$, where the bijection \mathcal{M} is a function between the RIS element indices

¹In this paper, we use $\bar{\Theta}$ to represent the diagonal phase shift matrix in the conventional RIS architecture, and use Θ to represent the non-diagonal phase shift matrix in our proposed RIS architecture. Θ is used when it is not specified which kind of RIS architecture is employed.

of incident signals and that of the reflected signals. For example, in Fig. 2 (a2), we consider an example using four elements, where the signal impinging on the first element is reflected from the second element, thus $\mathcal{M}(1) = 2$. Similarly, $\mathcal{M}(2) = 4$, $\mathcal{M}(3) = 3$, and $\mathcal{M}(4) = 1$. In Fig. 2 (b2), we consider an example using six elements, where the signal impinging on the first element is reflected from the third element, thus $\mathcal{M}(1) = 3$. Similarly, $\mathcal{M}(2) = 4$, $\mathcal{M}(3) = 1$, $\mathcal{M}(4) = 5$, $\mathcal{M}(5) = 2$, and $\mathcal{M}(6) = 6$.

Therefore, in our proposed method the phase shift matrix, denoted as $\tilde{\Theta}$, is non-diagonal, and there is only a single non-zero element in each row and each column. The phase shift matrix in Fig. 2 (a2) can be represented as

$$\tilde{\Theta} = \begin{bmatrix} 0 & 0 & 0 & e^{j\theta_{1,4}} \\ e^{j\theta_{2,1}} & 0 & 0 & 0 \\ 0 & 0 & e^{j\theta_{3,3}} & 0 \\ 0 & e^{j\theta_{4,2}} & 0 & 0 \end{bmatrix}. \quad (15)$$

Similarly, the phase shift matrix in Fig. 2 (b2) can be represented as

$$\tilde{\Theta} = \begin{bmatrix} 0 & 0 & e^{j\theta_{1,3}} & 0 & 0 & 0 \\ 0 & 0 & 0 & 0 & e^{j\theta_{2,5}} & 0 \\ e^{j\theta_{3,1}} & 0 & 0 & 0 & 0 & 0 \\ 0 & e^{j\theta_{4,2}} & 0 & 0 & 0 & 0 \\ 0 & 0 & 0 & e^{j\theta_{5,4}} & 0 & 0 \\ 0 & 0 & 0 & 0 & 0 & e^{j\theta_{6,6}} \end{bmatrix}. \quad (16)$$

Since only N non-zero entries of the phase shift matrix have to be optimized and N position information values of these non-zero entries have to be recorded in each coherence time for our RIS-aided systems, this only modestly increases the optimisation complexity and the amount of information transmitted over the BS-RIS controller link, compared to the conventional architecture.

Since the phase shift matrix in our proposed method is non-diagonal, we may refer to it as the *RIS architecture with non-diagonal phase shift matrix*. Compared to the conventional RIS architecture with diagonal phase shift matrix, the proposed non-diagonal phase shift matrix method has the potential of attaching higher channel gain. Let us consider an example using a 4-element RIS employed in a SISO system, and assume that the channel vector of the link from the BS to the RIS is $\mathbf{g} = [1.4e^{-j\frac{3\pi}{4}}, 0.2e^{j\frac{5\pi}{8}}, 0.4e^{-j\frac{7\pi}{8}}, 0.8e^{-j\frac{\pi}{8}}]^T$, while that of the link from the RIS to the user is $\mathbf{h}^H = [0.6e^{-j\frac{\pi}{4}}, 1e^{j\frac{2\pi}{3}}, 0.3e^{j\frac{\pi}{3}}, 0.1e^{j\frac{\pi}{8}}]$. In the conventional phase shift matrix based method, the channel gain can be maximized when the RIS phase shifts are designed coherently, i.e., $\theta_1 = -(\angle[\mathbf{g}]_1 + \angle[\mathbf{h}^H]_1) = \pi$, $\theta_2 = -(\angle[\mathbf{g}]_2 + \angle[\mathbf{h}^H]_2) = -\frac{3\pi}{2}$, $\theta_3 = -(\angle[\mathbf{g}]_3 + \angle[\mathbf{h}^H]_3) = \frac{5\pi}{8}$, $\theta_4 = -(\angle[\mathbf{g}]_4 + \angle[\mathbf{h}^H]_4) = \frac{\pi}{24}$. Then, the corresponding channel gain is given by $1.4 \times 0.6 + 0.2 \times 1 + 0.4 \times 0.3 + 0.8 \times 0.1 = 12.4$. By contrast, in our proposed non-diagonal phase shift matrix method, if the phase shift matrix is designed as the structure in (15), i.e. when the bijective function is $\mathcal{M}(1) = 2$, $\mathcal{M}(2) = 4$, $\mathcal{M}(3) = 3$, $\mathcal{M}(4) = 1$, and the RIS phase shifts are designed coherently, i.e., $\theta_{1,4} = -(\angle[\mathbf{g}]_4 + \angle[\mathbf{h}^H]_1) = \frac{5\pi}{12}$, $\theta_{2,1} = -(\angle[\mathbf{g}]_1 + \angle[\mathbf{h}^H]_2) = \frac{\pi}{12}$, $\theta_{3,3} = -(\angle[\mathbf{g}]_3 + \angle[\mathbf{h}^H]_3) = \frac{13\pi}{24}$, $\theta_{4,2} = -(\angle[\mathbf{g}]_2 + \angle[\mathbf{h}^H]_4) = -\frac{23\pi}{24}$, then the corresponding

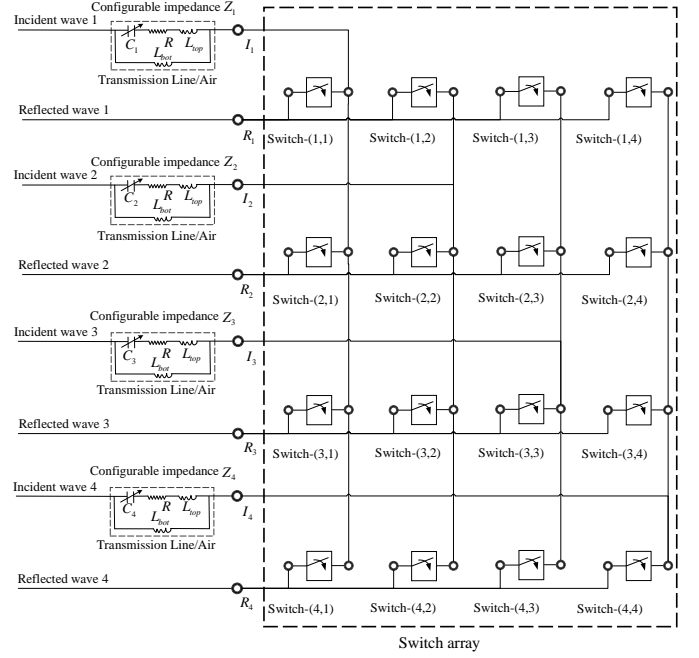


Fig. 3. The transmission line model of our proposed non-diagonal phase shift matrix architecture with $N = 4$ RIS elements.

channel gain is given by $0.8 \times 0.6 + 1.4 \times 1 + 0.4 \times 0.3 + 0.2 \times 0.1 = 20.2$. Therefore, higher channel gain can be achieved when the bijective function \mathcal{M} and the RIS phase shifts of the non-diagonal phase shift matrix are appropriately designed. The details of optimizing our proposed non-diagonal RIS phase shift matrix will be discussed in Section III, where the bijection function \mathcal{M} and the values of each element's phase shift can be obtained in the non-diagonal phase shift matrix $\tilde{\Theta}$.

C. Implementation Circuits

Although the implementational specifics of our proposed RIS architecture are beyond the scope of this paper, in the following we briefly highlight a potential implementation suitable for our proposed architecture.

In [24], the authors employed scattering parameter network models based on reciprocal architectures for describing the implementation of the conventional RIS structure and the fully-connected/group-connected RIS structure. The corresponding phase shift matrices are symmetric in [24]. On the other hand, our proposed architecture relies on a potentially non-symmetric matrix structure due to the fact that our design requires non-reciprocal connections.

In the following, we employ the classic transmission line model [27] for highlighting design the implementation of our proposed RIS architecture. The circuits of the conventional RIS architecture have been presented in [27], [28]. When it comes to using the transmission line model based design of our RIS architecture, we can employ switch arrays for connecting the different RIS elements. Fig. 3 illustrates an example of the transmission line model of our RIS architecture with $N = 4$ elements. In each RIS element, the reconfigurable impedance includes a bottom layer inductance L_{bot} , a top layer inductance L_{top} , an effective resistance R , and a variable capacitance C_n , where $n = 1, 2, \dots, N$ [28]. The phase shift of the reconfigurable impedance Z_n is controlled by its variable

capacitance C_n . To realize an N -element non-diagonal phase shift matrix, an array of $N \times N$ switches is required. The ON/OFF state of these switches is determined by the positions of non-zero entries in the RIS phase shift matrix. Specifically, the switches are turned on if the corresponding element in the RIS phase shift matrix is non zero, while they are turned off, if the corresponding elements are zero. For example, to realize the non-diagonal phase shift matrix of (15), Switch-(2,1), Switch-(4,2), Switch-(3,3) and Switch-(1,4) are turned on, while the other switches are turned off in Fig. 3. In this case, the signal impinging on the first RIS element is reflected from the second RIS element after phase shift configuration, while the signal impinging on the second RIS element is reflected from the fourth RIS element after phase shift configuration, etc. A potential implementation for the switches relies on using RF micro-electromechanical systems (MEMS) [29], which have been widely used in wireless communication systems as a benefit of their near-zero power consumption, high isolation, low insertion loss, low intermodulation products and low cost.

There are also other potential implementations for our proposed architecture. Explicitly, since we have to route the signal between the different elements depending on the bijection function \mathcal{M} , radio frequency couplers and isolators can be employed [30]–[33]. Additionally, passive phase shifters way also be employed in conjunction with these couplers for attaining accurate phase shifts [34]. Finally, the authors of [35], [36] provided comprehensive discussions of metasurfaces, including their operation and functionalities. Hence the proposed architecture is viable and has several existing implementations, which can be further optimized in our future researches.

III. BEAMFORMING DESIGN

In the previous section, we presented a novel RIS architecture, while here we present our joint beamforming design maximizing the attainable rate. This is achieved by jointly optimizing the passive beamforming matrix of the RIS and the TBF matrix of the BS. We start with deriving the closed-form solution of the SISO case, and then extend our analysis to more general single-user MISO case and multi-user MIMO case by employing the alternating optimization method and semi-definite relaxation technique [37], respectively.

A. Beamforming Design for SISO Systems

In SISO systems, both the BS and the single user are equipped with a single antenna, while the RIS has N reflecting elements. The system model in (10) can be written as

$$y = \sqrt{P_t} \mathbf{h}^H \Theta \mathbf{g} x + n, \quad (17)$$

where $x \in \mathbb{C}^{1 \times 1}$ is the transmitted signal, $\mathbf{g} \in \mathbb{C}^{N \times 1}$ is the channel vector arriving from the BS to the RIS, $\mathbf{h}^H \in \mathbb{C}^{1 \times N}$ is the channel vector of the link spanning from the RIS to the user, and $n \in \mathbb{C}^{1 \times 1}$ is the circularly symmetric complex Gaussian noise. The achievable rate of this SISO link is given by

$$R_{\text{SISO}} = \log_2 \left(1 + \frac{P_t}{\sigma_n^2} |\mathbf{h}^H \Theta \mathbf{g}|^2 \right). \quad (18)$$

Our aim is to find the phase shift matrix Θ that maximizes the rate, which can be formulated as

$$(P1.a) \quad \max_{\Theta} \log_2 \left(1 + \frac{P_t}{\sigma_n^2} |\mathbf{h}^H \Theta \mathbf{g}|^2 \right) \quad (19)$$

s.t. $0 \leq \theta_{\mathcal{M}(i),i} < 2\pi, \quad i = 1, 2, \dots, N.$

Similar to [25], by ignoring the constant terms, the achievable rate optimization problem of SISO systems is equivalent to maximizing the channel gain as follows

$$(P1.b) \quad \max_{\Theta} |\mathbf{h}^H \Theta \mathbf{g}|^2 \quad (20)$$

s.t. $0 \leq \theta_{\mathcal{M}(i),i} < 2\pi, \quad i = 1, 2, \dots, N.$

1) *Conventional RIS Architecture:* Again, in the conventional RIS architecture, the phase shift matrix is diagonal, so the bijection $f : I \rightarrow I'$ is essentially $\mathcal{M}(i) = i$. Therefore, the channel gain $|\mathbf{h}^H \bar{\Theta} \mathbf{g}|^2$ is given by

$$|\mathbf{h}^H \bar{\Theta} \mathbf{g}|^2 = \left(\sum_{i=1}^N [\mathbf{h}^H]_i [\mathbf{g}]_i e^{j\theta_i} \right)^2, \quad (21)$$

where the optimal solution for $\bar{\Theta}$ can be obtained as [25]

$$\theta_i = -(\angle[\mathbf{h}^H]_i + \angle[\mathbf{g}]_i), \quad i = 1, 2, \dots, N, \quad (22)$$

which essentially aligns all the signals reflected by the RIS with the impinging signals to arrange for their coherent combination, and the maximum channel gain based on (22) can be expressed as [25]

$$\max |\mathbf{h}^H \bar{\Theta} \mathbf{g}|^2 = \varrho_t \varrho_r \left(\sum_{i=1}^N a_i b_i \right)^2, \quad (23)$$

where a_i and b_i are the amplitude of $\frac{1}{\sqrt{\varrho_t}} [\mathbf{g}]_i$ and $\frac{1}{\sqrt{\varrho_r}} [\mathbf{h}^H]_i$, respectively. Observe from (23) that in conventional RIS architectures, the maximum channel gain is proportional to the square of the sum of $a_i b_i$, in which a_i and b_i are amalgamated based on the Equal Gain Combining (EGC) criterion.

2) *The proposed RIS Architecture:* Since in our proposed RIS architecture the signal impinging on the i th element can be reflected from the i' th element after phase shift adjustment, the channel gain can be written as

$$|\mathbf{h}^H \tilde{\Theta} \mathbf{g}|^2 = \left(\sum_{i=1}^N [\mathbf{h}^H]_{i'} [\mathbf{g}]_i e^{j\theta_{i',i}} \right)^2 = \varrho_t \varrho_r \left(\sum_{i=1}^N a_i b_{i'} \right)^2, \quad (24)$$

where

$$\theta_{i',i} = -(\angle[\mathbf{h}^H]_{i'} + \angle[\mathbf{g}]_i), \quad i = 1, 2, \dots, N, \quad i' = \mathcal{M}(i). \quad (25)$$

Hence, first we should aim for finding the function $\mathcal{M} : I \rightarrow I'$ to maximize the channel gain in (24). According to the Maximum Ratio Combining (MRC) criterion, the maximum of the channel gain in (24) is given by

$$\max |\mathbf{h}^H \tilde{\Theta} \mathbf{g}|^2 = \varrho_t \varrho_r \left(\sum_{i=1}^N a_{(i)} b_{(i)} \right)^2, \quad (26)$$

where $a_{(1)}, a_{(2)}, \dots, a_{(N)}$ represents the sequence of a_1, a_2, \dots, a_N sorted in an ascending order, and similarly, $b_{(1)}, b_{(2)}, \dots, b_{(N)}$ is the sequence of b_1, b_2, \dots, b_N sorted in an ascending order. According to [38], when a permutation matrix is multiplied from the left by a column vector, it will permute the elements of the column vector, while when

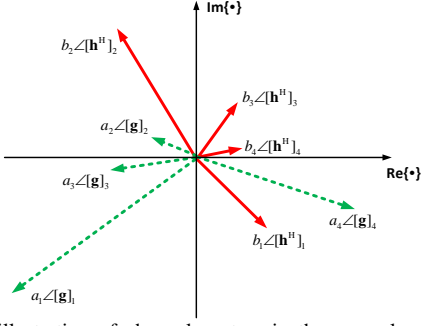


Fig. 4. The illustration of channel vectors in the example of a 4-element RIS-assisted system.

a permutation matrix is multiplied from the right by a row vector, it will permute the elements of the row vector. Therefore, the channel gain in (26) can be written as

$$\max |\mathbf{h}^H \tilde{\Theta} \mathbf{g}|^2 = |\mathbf{h}^H \mathbf{J}_r \tilde{\Theta} \mathbf{J}_t \mathbf{g}|^2, \quad (27)$$

where \mathbf{J}_t is a permutation matrix, which sorts the element amplitude in the column vector \mathbf{g} in an ascending order, yielding $\frac{1}{\sqrt{\varrho_t}} |\mathbf{J}_t \mathbf{g}| = [a_{(1)}, a_{(2)}, \dots, a_{(N)}]^T$. Still referring to (27), \mathbf{J}_r is a permutation matrix, which sorts the element amplitude in the row vector \mathbf{h}^H in an ascending order, leading to $\frac{1}{\sqrt{\varrho_r}} |\mathbf{h}^H \mathbf{J}_r| = [b_{(1)}, b_{(2)}, \dots, b_{(N)}]$. In this case, the channel vectors \mathbf{g} and \mathbf{h}^H can be combined based on the MRC criterion. Furthermore, $\tilde{\Theta}$ in (27) is a diagonal phase shift matrix, in which the i th diagonal element is given by

$$\theta_i = -(\angle[\mathbf{h}^H \mathbf{J}_r]_i + \angle[\mathbf{J}_t \mathbf{g}]_i), \quad i = 1, 2, \dots, N. \quad (28)$$

Therefore, the optimal non-diagonal phase matrix is formulated as $\tilde{\Theta}_{\text{opt}} = \mathbf{J}_r \tilde{\Theta} \mathbf{J}_t$.

To expound further, in Fig. 4, we present an example of a 4-element RIS-assisted system, where the ' \rightarrow ' vectors represent the BS-RIS channel vector \mathbf{g} , while the ' \rightarrow ' vectors correspond to the RIS-user channel vector \mathbf{h}^H . It can be observed that $a_2 < a_3 < a_4 < a_1$ and $b_4 < b_3 < b_1 < b_2$, so $a_{(1)} = a_2, a_{(2)} = a_3, a_{(3)} = a_4, a_{(4)} = a_1$, and $b_{(1)} = b_4, b_{(2)} = b_3, b_{(3)} = b_1, b_{(4)} = b_2$. Therefore, in our proposed architecture, the permutation matrices \mathbf{J}_t and \mathbf{J}_r are derived as

$$\mathbf{J}_t = \begin{bmatrix} 0 & 1 & 0 & 0 \\ 0 & 0 & 1 & 0 \\ 0 & 0 & 0 & 1 \\ 1 & 0 & 0 & 0 \end{bmatrix}, \quad \mathbf{J}_r = \begin{bmatrix} 0 & 0 & 1 & 0 \\ 0 & 0 & 0 & 1 \\ 0 & 1 & 0 & 0 \\ 1 & 0 & 0 & 0 \end{bmatrix}, \quad (29)$$

and the bijective function is given by $\mathcal{M}(1) = 2, \mathcal{M}(2) = 4, \mathcal{M}(3) = 3, \mathcal{M}(4) = 1$. Hence, the non-diagonal phase shift matrix $\tilde{\Theta}$ is designed as

$$\begin{aligned} \tilde{\Theta} &= \mathbf{J}_r \tilde{\Theta} \mathbf{J}_t \\ &= \mathbf{J}_r \cdot \text{diag}\{e^{j\theta_1}, e^{j\theta_2}, \dots, e^{j\theta_N}\} \cdot \mathbf{J}_t \\ &= \begin{bmatrix} 0 & 0 & 0 & e^{j\theta_3} \\ e^{j\theta_4} & 0 & 0 & 0 \\ 0 & 0 & e^{j\theta_2} & 0 \\ 0 & e^{j\theta_1} & 0 & 0 \end{bmatrix}, \end{aligned} \quad (30)$$

where $e^{j\theta_1} = e^{j\theta_{4,2}} = -(\angle[\mathbf{h}^H]_4 + \angle[\mathbf{g}]_2)$, $e^{j\theta_2} = e^{j\theta_{3,3}} = -(\angle[\mathbf{h}^H]_3 + \angle[\mathbf{g}]_3)$, $e^{j\theta_3} = e^{j\theta_{1,4}} = -(\angle[\mathbf{h}^H]_1 + \angle[\mathbf{g}]_4)$, $e^{j\theta_4} = e^{j\theta_{2,1}} = -(\angle[\mathbf{h}^H]_2 + \angle[\mathbf{g}]_1)$. Then, the corresponding channel gain is optimized as

$$|\mathbf{h}^H \tilde{\Theta} \mathbf{g}|^2 = \varrho_t \varrho_r (a_{(1)} b_{(1)} + a_{(2)} b_{(2)} + a_{(3)} b_{(3)} + a_{(4)} b_{(4)})^2$$

$$= \varrho_t \varrho_r (a_2 b_4 + a_3 b_3 + a_4 b_1 + a_1 b_2)^2. \quad (31)$$

We observe from (26) that in our proposed RIS architecture, the maximum channel gain is proportional to the square of the sum of $a_{(i)} b_{(i)}$, in which $a_{(i)}$ and $b_{(i)}$ are combined by obeying the MRC criterion, when the number of RIS elements N is large.

Finally, when the optimal phase shift matrix $\tilde{\Theta}_{\text{opt}}$ is attained, the achievable rate is given by

$$R_{\text{SISO}} = \log_2 \left(1 + \frac{P_t}{\sigma_n^2} |\mathbf{h}^H \tilde{\Theta}_{\text{opt}} \mathbf{g}|^2 \right). \quad (32)$$

B. Beamforming Design for Single-user MISO Systems

In single-user MISO systems, the BS is equipped with M downlink transmit antennas and the single user is equipped with a single receiver antenna, while the RIS has N elements. The system model in (10) can be written as

$$y = \sqrt{P_t} \mathbf{h}^H \tilde{\Theta} \mathbf{G} \mathbf{w} x + n, \quad (33)$$

and the achievable rate is given by

$$R_{\text{MISO}} = \log_2 \left(1 + \frac{P_t}{\sigma_n^2} |\mathbf{h}^H \tilde{\Theta} \mathbf{G} \mathbf{w}|^2 \right). \quad (34)$$

The problem of maximizing the achievable rate can be formulated as

$$(P2.a) \quad \max_{\tilde{\Theta}, \mathbf{w}} \log_2 \left(1 + \frac{P_t}{\sigma_n^2} |\mathbf{h}^H \tilde{\Theta} \mathbf{G} \mathbf{w}|^2 \right) \quad (35)$$

$$\text{s.t.} \quad \|\mathbf{w}\| = 1,$$

$$0 \leq \theta_{\mathcal{M}(i),i} < 2\pi, \quad i = 1, 2, \dots, N.$$

Similar to SISO cases, the achievable rate optimization problem of single-user MISO systems is equivalent to maximizing the channel gain as follows

$$(P2.b) \quad \max_{\tilde{\Theta}, \mathbf{w}} |\mathbf{h}^H \tilde{\Theta} \mathbf{G} \mathbf{w}|^2 \quad (36)$$

$$\text{s.t.} \quad \|\mathbf{w}\| = 1,$$

$$0 \leq \theta_{\mathcal{M}(i),i} < 2\pi, \quad i = 1, 2, \dots, N.$$

Since (P2.b) represents a non-convex problem, we employ the popular alternating optimization method for solving it iteratively.

Firstly, when the TBF vector \mathbf{w} is given, $\mathbf{G} \mathbf{w}$ becomes a column vector, and the phase shift matrix $\tilde{\Theta}$ can be designed similarly as in the SISO case.

Secondly, when the phase shift matrix $\tilde{\Theta}$ is given, the equivalent channel can be obtained as $\mathbf{h}^H \tilde{\Theta} \mathbf{G}$. Then the TBF vector can be designed based on the maximum ratio transmission (MRT) method, yielding $\mathbf{w} = \frac{(\mathbf{h}^H \tilde{\Theta} \mathbf{G})^H}{\|\mathbf{h}^H \tilde{\Theta} \mathbf{G}\|}$. The detailed process of the alternating optimization method conceived for RIS-assisted single-user MISO systems is shown in Algorithm 1.

When the optimal phase shift matrix $\tilde{\Theta}_{\text{opt}}$ and TBF vector \mathbf{w}_{opt} are obtained, the achievable rate is given by

$$R_{\text{MISO}} = \log_2 \left(1 + \frac{P_t}{\sigma_n^2} |\mathbf{h}^H \tilde{\Theta}_{\text{opt}} \mathbf{G} \mathbf{w}_{\text{opt}}|^2 \right). \quad (37)$$

C. Beamforming Design for Multi-user MIMO Systems

In multi-user MIMO systems, including a BS having M transmit antennas and K single-antenna users, the system model is given by

$$y = \sqrt{P_t} \mathbf{H} \tilde{\Theta} \mathbf{G} \mathbf{W} \sqrt{\Lambda} \mathbf{x} + \mathbf{n}, \quad (38)$$

Algorithm 1 Alternating optimization method for RIS-assisted single-user MISO systems

Input: BS-RIS channel matrix \mathbf{G} , and RIS-user channel vector \mathbf{h}^H .

Output: The optimal phase shift matrix $\tilde{\Theta}_{\text{opt}}$, and the optimal transmission beamforming vector \mathbf{w}_{opt} .

- 1: Choose the proper permutation matrix \mathbf{J}_r which sorts the element amplitude of row vector \mathbf{h}^H in an ascending order.
- 2: Set an initial \mathbf{w} satisfying $\|\mathbf{w}\| = 1$.
- 3: **Repeat**
- 4: Choose the proper permutation matrix \mathbf{J}_t which can sort the element amplitude of column vector $\mathbf{G}\mathbf{w}$ in an ascending order.
- 5: According to the row vector $\mathbf{h}^H\mathbf{J}_r$ and column vector $\mathbf{J}_t\mathbf{G}\mathbf{w}$, the elements in diagonal matrix $\tilde{\Theta}$ is designed as $\theta_i = -(\angle[\mathbf{h}^H\mathbf{J}_r]_i + \angle[\mathbf{J}_t\mathbf{G}\mathbf{w}]_i)$, $i = 1, 2, \dots, N$.
- 6: Design the transmission beamforming vector based on MRT criterion as $\mathbf{w} = \frac{(\mathbf{h}^H\mathbf{J}_r\tilde{\Theta}\mathbf{J}_t\mathbf{G})^H}{\|\mathbf{h}^H\mathbf{J}_r\tilde{\Theta}\mathbf{J}_t\mathbf{G}\|}$.
- 7: **Until** reaching the maximal number of iterations or the increment of the objective value is smaller than threshold ϵ .
- 8: **Return** the optimal phase shift matrix $\tilde{\Theta}_{\text{opt}} = \mathbf{J}_r\tilde{\Theta}\mathbf{J}_t$ and the optimal transmission beamforming vector $\mathbf{w}_{\text{opt}} = \frac{(\mathbf{h}^H\tilde{\Theta}\mathbf{G})^H}{\|\mathbf{h}^H\tilde{\Theta}\mathbf{G}\|}$.

and the achievable rate is formulated as

$$R_{\text{MIMO}} = \log_2 \left| \mathbf{I} + \frac{P_t}{\sigma_n^2} \mathbf{H}\tilde{\Theta}\mathbf{G}\mathbf{W}\mathbf{A}\mathbf{W}^H\mathbf{G}^H\tilde{\Theta}^H\mathbf{H}^H \right|. \quad (39)$$

The problem of maximizing the achievable rate can be formulated as

$$(P3.a) \quad \max_{\mathbf{w}, \tilde{\Theta}, \mathbf{A}} \log_2 \left| \mathbf{I} + \frac{P_t}{\sigma_n^2} \mathbf{H}\tilde{\Theta}\mathbf{G}\mathbf{W}\mathbf{A}\mathbf{W}^H\mathbf{G}^H\tilde{\Theta}^H\mathbf{H}^H \right| \quad (40)$$

s.t. $\|\mathbf{w}_k\| = 1$, $k = 1, 2, \dots, K$,

$\lambda_1 + \lambda_2 + \dots + \lambda_K = 1$,

$0 \leq \theta_{\mathcal{M}(i),i} < 2\pi$, $i = 1, 2, \dots, N$.

According to [12], the two-stage algorithm, which decouples the joint beamforming design problem (P3.a) into two sub-problems, has lower computational complexity, while suffering from a slight performance erosion, when compared to alternating optimization algorithm. Therefore, we employ the two-stage algorithm for maximizing the achievable rate of our proposed RIS architecture as follows.

- *Stage I:* The RIS phase shift matrix is optimized by maximizing the sum of the combined channel gain of all users, which can be expressed as

$$(P3.b1) \quad \max_{\tilde{\Theta}} \sum_{k=1}^K \|\mathbf{h}_k^H \tilde{\Theta} \mathbf{G}\|^2 \quad (41)$$

s.t. $0 \leq \theta_{\mathcal{M}(i),i} < 2\pi$, $i = 1, 2, \dots, N$.

We employ the SDR method for solving the problem (P3.b1). Specifically, let us define a column vector $\mathbf{q} = [e^{j\theta_1}, e^{j\theta_2}, \dots, e^{j\theta_N}]^H$. Then $\sum_{k=1}^K \|\mathbf{h}_k^H \tilde{\Theta} \mathbf{G}\|^2$ can be represented as

$$\begin{aligned} \sum_{k=1}^K \|\mathbf{h}_k^H \tilde{\Theta} \mathbf{G}\|^2 &= \sum_{k=1}^K \|\mathbf{h}_k^H \mathbf{J}_r \tilde{\Theta} \mathbf{J}_t \mathbf{G}\|^2 \\ &= \sum_{k=1}^K \|\mathbf{q}^H \text{diag}\{\mathbf{h}_k^H \mathbf{J}_r\} \mathbf{J}_t \mathbf{G}\|^2 \end{aligned}$$

$$\begin{aligned} &= \sum_{k=1}^K \mathbf{q}^H \Phi_k \Phi_k^H \mathbf{q} \\ &= \mathbf{q}^H \left(\sum_{k=1}^K \Phi_k \Phi_k^H \right) \mathbf{q}, \end{aligned} \quad (42)$$

where $\Phi_k = \text{diag}\{\mathbf{h}_k^H \mathbf{J}_r\} \mathbf{J}_t \mathbf{G}$. Since the phase shift matrix $\tilde{\Theta}$ is determined by \mathbf{q} , \mathbf{J}_t and \mathbf{J}_r , the problem of maximizing $\sum_{k=1}^K \|\mathbf{h}_k^H \tilde{\Theta} \mathbf{G}\|^2$ is formulated as

$$(P3.b2) \quad \max_{\mathbf{q}, \mathbf{J}_t, \mathbf{J}_r} \mathbf{q}^H \left(\sum_{k=1}^K \Phi_k \Phi_k^H \right) \mathbf{q} \quad (43)$$

s.t. $|\mathbf{q}_i| = 1$, $i = 1, 2, \dots, N$.

In Φ_k , since the BS-RIS channel matrix $\mathbf{G} = [\mathbf{g}_1, \mathbf{g}_2, \dots, \mathbf{g}_M]$ has M columns, and the RIS-users' channel matrix $\mathbf{h} = [\mathbf{h}_1, \mathbf{h}_2, \dots, \mathbf{h}_K]^H$ has K rows, the permutation matrices \mathbf{J}_t and \mathbf{J}_r cannot be designed similarly to the SISO case by using a sorting method. Although the optimal permutation matrices \mathbf{J}_t and \mathbf{J}_r can be found by exhaustive search, we resort to the following sub-optimal method for reducing the search complexity. We introduce the notation of $\mathbf{g}' = \frac{1}{M} \sum_{m=1}^M |\mathbf{g}_m|$, and $\mathbf{h}' = \frac{1}{K} \sum_{k=1}^K |\mathbf{h}_k|$. Then, we choose the permutation matrix \mathbf{J}_t which sorts the column vector \mathbf{g}' in an ascending order, and the permutation matrix \mathbf{J}_r , which sorts the row vector \mathbf{h}'^H in an ascending order.

After the permutation matrices \mathbf{J}_t and \mathbf{J}_r are determined, (P3.b2) becomes a non-convex quadratically constrained quadratic program (QCQP), and it can be solved by defining $\mathbf{Q} = \mathbf{q}\mathbf{q}^H$, which needs to satisfy that $\mathbf{Q} \succeq 0$ and $\text{Rank}(\mathbf{Q}_{\text{opt}}) = 1$. Since the rank-one constraint is non-convex, we relax this constraint [12] and (P3.b2) can be translated into a standard convex SDR problem as follows

$$(P3.b3) \quad \max_{\mathbf{Q}} \text{Tr} \left(\left(\sum_{k=1}^K \Phi_k \Phi_k^H \right) \mathbf{Q} \right) \quad (44)$$

s.t. $\mathbf{Q} \succeq 0$,

$|\mathbf{Q}_{i,i}| = 1$, $i = 1, 2, \dots, N$.

The optimal solution, denoted as \mathbf{Q}_{opt} , in (P3.b3) can be found by using CVX [39]. If $\text{Rank}(\mathbf{Q}_{\text{opt}}) > 1$, the optimal solution of \mathbf{q} , denoted as \mathbf{q}_{opt} , can be recovered from \mathbf{Q}_{opt} by eigenvalue decomposition as $\mathbf{q}_{\text{opt}} = \sqrt{\nu_1} \mathbf{q}_1$, in which ν_1 is the largest eigenvalue of the matrix \mathbf{Q}_{opt} , and \mathbf{q}_1 is the corresponding eigenvector. After obtaining the permutation matrix \mathbf{J}_t , \mathbf{J}_r and \mathbf{q}_{opt} , the optimal phase shift matrix, denoted as $\tilde{\Theta}_{\text{opt}}$, can be derived as $\tilde{\Theta}_{\text{opt}} = \mathbf{J}_r \text{diag}\{\mathbf{q}_{\text{opt}}^H\} \mathbf{J}_t$.

- *Stage II:* When the optimal phase shift matrix is obtained in the first stage, the equivalent channel can be represented as $\mathbf{H}_{\text{equ}} = \mathbf{H}^H \tilde{\Theta}_{\text{opt}} \mathbf{G}$. Upon using the SVD method, the equivalent channel can be expressed as $\mathbf{H}_{\text{equ}} = \mathbf{U}\mathbf{\Sigma}\mathbf{V}^H$. The TBF matrix \mathbf{W} is designed as $\mathbf{W}_{\text{opt}} = \mathbf{V}^{(1:K)}$, where $\mathbf{V}^{(1:K)}$ represents the first K columns of the right singular matrix \mathbf{V} . Afterwards, the power allocation matrix $\mathbf{\Lambda}$ is designed by the popular water-filling method [40], based on the optimized equivalent channel \mathbf{H}_{equ} and the optimized TBF matrix \mathbf{W}_{opt} .

Finally, the achievable rate can be represented as

$$R_{\text{MIMO}} = \log_2 \left(\mathbf{I} + \frac{P_t}{\sigma_n^2} \mathbf{H}_{\text{equ}} \mathbf{C} \mathbf{H}_{\text{equ}}^H \right), \quad (45)$$

where $\mathbf{C} = \mathbf{W}_{\text{opt}} \mathbf{A} \mathbf{W}_{\text{opt}}^H$ is the transmit covariance matrix.

IV. THEORETICAL ANALYSIS

In this section, to highlight the channel gain enhancement in our proposed method compared with the conventional diagonal phase shift matrix method, we present the theoretical analysis of our proposed RIS architecture designed for the SISO systems. Firstly, we analyze the scaling law of our proposed RIS architecture relying on a non-diagonal phase matrix to derive the channel gain in Rician channels. Then, we discuss some special cases for different Rician factor values. Afterwards, we present the instantaneous SNR, as well as the outage probability and the average BER, of our proposed non-diagonal phase shift matrix based RIS systems in Rayleigh fading channels. Finally, the complexity comparison of the conventional RIS architecture and our proposed RIS architecture is presented.

A. Channel Gain Analysis

To compare the fundamental limit of the conventional RIS architecture and of our proposed RIS architecture, we quantify the channel gain as a function of the number of RIS reflecting elements N .

In the SISO system, the BS-RIS channel vector and RIS-user channel vector are given by

$$\mathbf{g} = \sqrt{\frac{\kappa_{\mathbf{g}}}{1 + \kappa_{\mathbf{g}}}} \bar{\mathbf{g}} + \sqrt{\frac{1}{1 + \kappa_{\mathbf{g}}}} \tilde{\mathbf{g}}, \quad (46)$$

$$\mathbf{h}^H = \sqrt{\frac{\kappa_{\mathbf{h}}}{1 + \kappa_{\mathbf{h}}}} \bar{\mathbf{h}}_r^H + \sqrt{\frac{1}{1 + \kappa_{\mathbf{h}}}} \tilde{\mathbf{h}}_r^H, \quad (47)$$

where $\kappa_{\mathbf{g}}$ and $\kappa_{\mathbf{h}}$ represent the Rician factors of BS-RIS path and RIS-user path, respectively. Since a_i is the amplitudes of $\frac{1}{\sqrt{\varrho_t}} [\mathbf{g}]_i$, a_i follows the Rice distribution with noncentrality parameter $\nu = \sqrt{\frac{\kappa_{\mathbf{g}}}{1 + \kappa_{\mathbf{g}}}}$ and scale parameter $\sigma = \sqrt{\frac{1}{2(1 + \kappa_{\mathbf{g}})}}$, with the PDF and CDF as [41]

$$f_{a_i}(x) = 2(1 + \kappa_{\mathbf{g}}) x e^{-(1 + \kappa_{\mathbf{g}})x^2 - \kappa_{\mathbf{g}}} I_0 \left(2\sqrt{\kappa_{\mathbf{g}}(1 + \kappa_{\mathbf{g}})} x \right), \quad (48)$$

$$F_{a_i}(x) = 1 - Q_1 \left(\sqrt{2\kappa_{\mathbf{g}}}, \sqrt{2(1 + \kappa_{\mathbf{g}})} x \right), \quad (49)$$

where $I_0(\cdot)$ is the modified Bessel function of the first kind with order zero, and $Q_1(\cdot)$ is the Marcum Q-function [41]. Similarly, since b_i is the amplitude of $\frac{1}{\sqrt{\varrho_r}} [\mathbf{h}^H]_i$, b_i follows Rice distribution with noncentrality parameter $\nu = \sqrt{\frac{\kappa_{\mathbf{h}}}{1 + \kappa_{\mathbf{h}}}}$ and scale parameter $\sigma = \sqrt{\frac{1}{2(1 + \kappa_{\mathbf{h}})}}$, with the PDF and CDF as

$$f_{b_i}(x) = 2(1 + \kappa_{\mathbf{h}}) x e^{-(1 + \kappa_{\mathbf{h}})x^2 - \kappa_{\mathbf{h}}} I_0 \left(2\sqrt{\kappa_{\mathbf{h}}(1 + \kappa_{\mathbf{h}})} x \right), \quad (50)$$

$$F_{b_i}(x) = 1 - Q_1 \left(\sqrt{2\kappa_{\mathbf{h}}}, \sqrt{2(1 + \kappa_{\mathbf{h}})} x \right). \quad (51)$$

Since in a Rice distribution $\text{Rice}(\nu, \sigma)$, the first moment and second moment are $\sigma \sqrt{\pi/2} L_{1/2}(-\nu^2/2\sigma^2)$ and $\nu^2 + 2\sigma^2$ respectively [41], in which $L_{1/2}(\cdot)$ is the Laguerre polynomial, we can get that [41]

$$\mathbb{E}(a_i) = \sqrt{\frac{\pi}{4(1 + \kappa_{\mathbf{g}})}} L_{\frac{1}{2}}(-\kappa_{\mathbf{g}}), \quad (52)$$

$$\mathbb{E}(b_i) = \sqrt{\frac{\pi}{4(1 + \kappa_{\mathbf{h}})}} L_{\frac{1}{2}}(-\kappa_{\mathbf{h}}), \quad (53)$$

$$\mathbb{E}(a_i^2) = \mathbb{E}(b_i^2) = 1, \quad (54)$$

1) *Average channel gain in the conventional RIS architecture:* In SISO systems, the average channel gain of the conventional RIS architecture relying on the diagonal phase shift matrix, denoted as \mathbf{g}_{diag} , when considering Rician fading channel, is given by

$$\begin{aligned} \mathbf{g}_{\text{diag}} &= \mathbb{E}(|\mathbf{h}^H \mathbf{\Theta} \mathbf{g}|^2) \\ &= \mathbb{E} \left(\left(\sum_{i=1}^N |[\mathbf{g}]_i| |[\mathbf{h}^H]_i| \right)^2 \right) \\ &= \varrho_t \varrho_r \mathbb{E} \left(\left(\sum_{i=1}^N a_i b_i \right)^2 \right) \\ &= \varrho_t \varrho_r \left(\sum_{i=1}^N \mathbb{E}(a_i^2) \mathbb{E}(b_i^2) \right. \\ &\quad \left. + 2 \sum_{i=1}^{N-1} \sum_{j=i+1}^N \mathbb{E}(a_i) \mathbb{E}(b_i) \mathbb{E}(a_j) \mathbb{E}(b_j) \right). \end{aligned} \quad (55)$$

According to (52), (53), (54) and (55), we can get

$$\mathbf{g}_{\text{diag}} = \varrho_t \varrho_r \left(N + \frac{\pi^2}{16} N(N-1) \frac{L_{\frac{1}{2}}^2(-\kappa_{\mathbf{g}}) L_{\frac{1}{2}}^2(-\kappa_{\mathbf{h}})}{(\kappa_{\mathbf{g}} + 1)(\kappa_{\mathbf{h}} + 1)} \right). \quad (56)$$

2) *Average channel gain analysis in the proposed RIS architecture:* Since $a_{(1)}, a_{(2)}, \dots, a_{(N)}$ and $b_{(1)}, b_{(2)}, \dots, b_{(N)}$ represent the sequences of a_1, a_2, \dots, a_N and b_1, b_2, \dots, b_N sorted in an ascending order, the average channel gain of the proposed RIS architecture having a non-diagonal phase shift matrix, denoted as $\mathbf{g}_{\text{nonnd}}$, can be expressed as

$$\begin{aligned} \mathbf{g}_{\text{nonnd}} &= \mathbb{E}(|\mathbf{h}^H \mathbf{J}_r \mathbf{\Theta} \mathbf{J}_t \mathbf{g}|^2) \\ &= \varrho_t \varrho_r \mathbb{E} \left(\left(\sum_{i=1}^N a_{(i)} b_{(i)} \right)^2 \right) \\ &= \varrho_t \varrho_r \left(\sum_{i=1}^N \mathbb{E}(a_{(i)}^2) \mathbb{E}(b_{(i)}^2) \right. \\ &\quad \left. + 2 \sum_{i=1}^{N-1} \sum_{j=i+1}^N \mathbb{E}(a_{(i)}) \mathbb{E}(b_{(i)}) \mathbb{E}(a_{(j)}) \mathbb{E}(b_{(j)}) \right). \end{aligned} \quad (57)$$

According to the order statistic theory [42], we can get the PDF of $a_{(i)}$ and $b_{(i)}$ as

$$f_{a_{(i)}}(x) = C_{i,N} [F_{a_i}(x)]^{i-1} [1 - F_{a_i}(x)]^{N-i} f_{a_i}(x), \quad (58)$$

$$f_{b_{(i)}}(x) = C_{i,N} [F_{b_i}(x)]^{i-1} [1 - F_{b_i}(x)]^{N-i} f_{b_i}(x), \quad (59)$$

where $f_{a_i}(x)$, $F_{a_i}(x)$, $f_{b_i}(x)$ and $F_{b_i}(x)$ are given in (48), (49), (50) and (51), respectively, and $C_{i,N} = \frac{N!}{(i-1)!(N-i)!}$.

Therefore, the first moment of $a_{(i)}$ is given by

$$\begin{aligned}\mathbb{E}(a_{(i)}) &= \int_0^\infty x f_{a_{(i)}}(x) dx \\ &= \int_0^\infty x C_{i,N} [F_{a_i}(x)]^{i-1} [1 - F_{a_i}(x)]^{N-i} f_{a_i}(x) dx.\end{aligned}\quad (60)$$

Substituting (48) and (49) into (60), we can get

$$\begin{aligned}\mathbb{E}(a_{(i)}) &= \frac{C_{i,N} e^{-\kappa_g}}{\sqrt{2(1+\kappa_g)}} \int_0^\infty x^2 e^{-\frac{x^2}{2}} I_0(\sqrt{2\kappa_g}x) \times \\ &\quad [1 - Q_1(\sqrt{2\kappa_g}, x)]^{i-1} [Q_1(\sqrt{2\kappa_g}, x)]^{N-i} dx.\end{aligned}\quad (61)$$

Similarly, we can get the second moment of $a_{(i)}$, the first moment of $b_{(i)}$, and the second moment of $b_{(i)}$ as

$$\begin{aligned}\mathbb{E}(a_{(i)}^2) &= \int_0^\infty x^2 f_{a_{(i)}}(x) dx \\ &= \frac{C_{i,N} e^{-\kappa_g}}{2(1+\kappa_g)} \int_0^\infty x^3 e^{-\frac{x^2}{2}} I_0(\sqrt{2\kappa_g}x) \times \\ &\quad [1 - Q_1(\sqrt{2\kappa_g}, x)]^{i-1} [Q_1(\sqrt{2\kappa_g}, x)]^{N-i} dx,\end{aligned}\quad (62)$$

$$\begin{aligned}\mathbb{E}(b_{(i)}) &= \int_0^\infty x f_{b_{(i)}}(x) dx \\ &= \frac{C_{i,N} e^{-\kappa_h}}{\sqrt{2(1+\kappa_h)}} \int_0^\infty x^2 e^{-\frac{x^2}{2}} I_0(\sqrt{2\kappa_h}x) \times \\ &\quad [1 - Q_1(\sqrt{2\kappa_h}, x)]^{i-1} [Q_1(\sqrt{2\kappa_h}, x)]^{N-i} dx,\end{aligned}\quad (63)$$

$$\begin{aligned}\mathbb{E}(b_{(i)}^2) &= \int_0^\infty x^2 f_{b_{(i)}}(x) dx \\ &= \frac{C_{i,N} e^{-\kappa_h}}{2(1+\kappa_h)} \int_0^\infty x^3 e^{-\frac{x^2}{2}} I_0(\sqrt{2\kappa_h}x) \times \\ &\quad [1 - Q_1(\sqrt{2\kappa_h}, x)]^{i-1} [Q_1(\sqrt{2\kappa_h}, x)]^{N-i} dx.\end{aligned}\quad (64)$$

Substituting (61), (62), (63) and (64) into (57), we can get the average channel gain of the proposed RIS architecture $\mathfrak{g}_{\text{non-d}}$.

B. Effect of the Value of the Rician Factor on the Channel Gain

To get deep insights on the effects of the Rician factors κ_g and κ_h on the channel gain, we investigate the following cases.

Case I, $\kappa_g \rightarrow \infty$ (or $\kappa_h \rightarrow \infty$): In this case, the BS-RIS channel (or RIS-user channel) is fully dominated by the LoS path, the conventional RIS architecture and our proposed RIS architecture get the same average channel gain as

$$\mathfrak{g}_{\text{diag}} = \mathfrak{g}_{\text{non-d}}. \quad (65)$$

Proof: See Appendix A. ■

Furthermore, when $\kappa_g \rightarrow \infty$ and $\kappa_h \rightarrow \infty$ simultaneously, both the conventional RIS architecture and our proposed RIS architecture gets the channel gain upper bound as

$$\mathfrak{g}_{\text{diag}} = \mathfrak{g}_{\text{non-d}} = \varrho_t \varrho_r N^2. \quad (66)$$

This can be easily observed since $a_i = 1$ and $b_i = 1$ for all $i = 1, 2, \dots, N$ when $\kappa_g \rightarrow \infty$ and $\kappa_h \rightarrow \infty$.

Case II, $\kappa_g = 0$ and $\kappa_h = 0$: In this case, the BS-RIS channel and RIS-user channel experience Rayleigh fading. The average channel gain of the conventional RIS architecture $\mathfrak{g}_{\text{diag}}$ and the proposed non-diagonal RIS architecture $\mathfrak{g}_{\text{non-d}}$ are derived as follows.

- *Average channel gain in the conventional RIS architecture:* When $\kappa_g = 0$ and $\kappa_h = 0$, a_i and b_i both follow the Rayleigh distribution associated with the scaling parameter $\sigma = \frac{\sqrt{2}}{2}$, and a_i^2 and b_i^2 obey the exponential distribution having the rate parameter of $\lambda = 1$. Therefore,

$$\mathbb{E}(a_i) = \mathbb{E}(b_i) = \frac{\sqrt{\pi}}{2}, \quad (67)$$

$$\mathbb{E}(a_i^2) = \mathbb{E}(b_i^2) = 1. \quad (68)$$

Substituting (67) and (68) into (55), we can get

$$\mathfrak{g}_{\text{diag}} = \varrho_t \varrho_r \left(N + N(N-1) \frac{\pi^2}{16} \right). \quad (69)$$

- *Average channel gain in the proposed RIS architecture:* Since a_i and b_i both follow Rayleigh distribution associated with the scaling parameter $\sigma = \frac{\sqrt{2}}{2}$, $a_{(i)}$ and $b_{(i)}$ are also identically distributed. Therefore, (57) can be simplified as

$$\begin{aligned}\mathfrak{g}_{\text{non-d}} &= \varrho_t \varrho_r \left(\sum_{i=1}^N (\mathbb{E}(a_{(i)}^2))^2 \right. \\ &\quad \left. + 2 \sum_{i=1}^{N-1} \sum_{j=i+1}^N (\mathbb{E}(a_{(i)}))^2 (\mathbb{E}(a_{(j)}))^2 \right).\end{aligned}\quad (70)$$

Note that $a_1^2, a_2^2, \dots, a_N^2$ independently follow the exponential distribution having the rate parameter $\lambda = 1$, and given the lemma in [42] that

$$a_{(i)}^2 = \sum_{k=1}^i \frac{Z_k}{N-k+1}, \quad i = 1, 2, \dots, N, \quad (71)$$

where the random variable Z_k follows the exponential distribution with the rate parameter $\lambda = 1$, we arrive at:

$$\sum_{i=1}^N (\mathbb{E}(a_{(i)}^2))^2 = \sum_{i=1}^N \left(\sum_{k=1}^i \frac{1}{N-k+1} \right)^2. \quad (72)$$

To derive $\sum_{i=1}^{N-1} \sum_{j=i+1}^N (\mathbb{E}(a_{(i)}))^2 (\mathbb{E}(a_{(j)}))^2$, firstly, we present the following *Theorem 1*.

Theorem 1. The PDF of $a_{(i)}$ is given by a linear combination of the PDF of i Rayleigh distributions having the scaling parameter $\sigma = \frac{1}{\sqrt{2(N-i+k+1)}}$. Specifically, the PDF of $a_{(i)}$ can be written as

$$\begin{aligned}f_{a_{(i)}}(x) &= \sum_{k=0}^{i-1} \binom{N}{i-k-1} \binom{N-i+k}{k} (-1)^k \\ &\quad f_X \left(x; \sigma = \frac{1}{\sqrt{2(N-i+k+1)}} \right),\end{aligned}\quad (73)$$

where $f_X(x; \sigma)$ is the PDF of a random variable X following the Rayleigh distribution having the scaling parameter σ .

Proof: See Appendix B. ■

Since the mean of $f_X(x; \sigma)$ equals $\sigma \sqrt{\frac{\pi}{2}}$, then

$$\begin{aligned}\mathbb{E} \left(f_X(x; \sigma = \frac{1}{\sqrt{2(N-i+k+1)}}) \right) \\ = \frac{\sqrt{\pi}}{2} \frac{1}{\sqrt{N-i+k+1}}.\end{aligned}\quad (74)$$

Upon combining (73) and (74), we arrive at:

$$\mathbb{E} [f_{a(i)}(x)] = \frac{\sqrt{\pi}}{2} \sum_{k=0}^{i-1} \binom{N}{i-k-1} \binom{N-i+k}{k} (-1)^k \frac{1}{\sqrt{N-i+k+1}}. \quad (75)$$

Therefore, $\sum_{i=1}^{N-1} \sum_{j=i+1}^N [\mathbb{E}(a(i))]^2 [\mathbb{E}(a(j))]^2$ is obtained as

$$\begin{aligned} \sum_{i=1}^{N-1} \sum_{j=i+1}^N (\mathbb{E}(a(i)))^2 (\mathbb{E}(a(j)))^2 &= \frac{\pi^2}{16} \sum_{i=1}^{N-1} \sum_{j=i+1}^N \\ &\left[\sum_{k=0}^{i-1} (-1)^k \binom{N}{i-k-1} \binom{N-i+k}{k} \frac{1}{\sqrt{N-i+k+1}} \right]^2 \\ &\left[\sum_{k=0}^{j-1} (-1)^k \binom{N}{j-k-1} \binom{N-j+k}{k} \frac{1}{\sqrt{N-j+k+1}} \right]^2. \end{aligned} \quad (76)$$

According to (70), (72) and (76), we get the theoretical result of the channel gain $\mathfrak{g}_{\text{nonnd}}$ as

$$\begin{aligned} \mathfrak{g}_{\text{nonnd}} &= \varrho_t \varrho_r \sum_{i=1}^N \left(\sum_{k=1}^i \frac{1}{N-k+1} \right)^2 + \varrho_t \varrho_r \frac{\pi^2}{8} \sum_{i=1}^{N-1} \sum_{j=i+1}^N \\ &\left[\sum_{k=0}^{i-1} \binom{N}{i-k-1} \binom{N-i+k}{k} (-1)^k \frac{1}{\sqrt{N-i+k+1}} \right]^2 \\ &\left[\sum_{k=0}^{j-1} \binom{N}{j-k-1} \binom{N-j+k}{k} (-1)^k \frac{1}{\sqrt{N-j+k+1}} \right]^2. \end{aligned} \quad (77)$$

Upon comparing (55) to (57), we can find that the channel gain of the conventional RIS architecture is proportional to the expectation of the square of $a_1 b_1 + a_2 b_2 + \dots + a_N b_N$, while the channel gain of our proposed RIS architecture is proportional to the expectation of the square of $a_{(1)} b_{(1)} + a_{(2)} b_{(2)} + \dots + a_{(N)} b_{(N)}$. Therefore, in conventional RIS architectures the channel gain is proportional to the equal gain combination of the channel parameters, while in our proposed RIS architecture the channel gain is proportional to the maximum ratio combination of the channel parameters, when the number of RIS elements N is large.

We define the *normalized channel gain* $\hat{\mathfrak{g}}$ as the average channel gain \mathfrak{g} normalized by the upper bound of $\varrho_t \varrho_r N^2$ in LoS channels, i.e. $\hat{\mathfrak{g}} = \frac{\mathfrak{g}}{\varrho_t \varrho_r N^2}$. In Fig. 5, we present the normalized power gain of our proposed RIS architecture, compared to that of the fully-connected/group-connected RIS architecture of [24] in Rayleigh fading channels, i.e. $\kappa_{\mathbf{g}} = \kappa_{\mathbf{h}} = 0$, where G represents the group size of a group-connected RIS architecture. Fig. 5 shows that when the number of RIS elements is small, the power gain of our proposed RIS architecture is worse than that of the fully connected RIS architecture of [24]. However, the performance of our proposed RIS architecture becomes better than that of the group-connected RIS architecture and approaches that of the fully-connected RIS architecture upon increasing the number of RIS

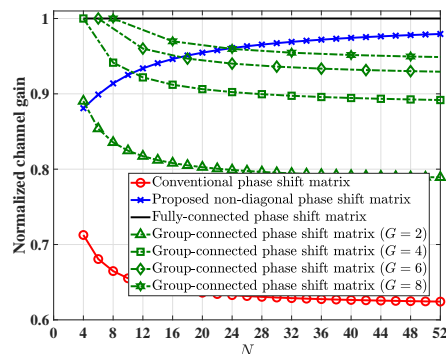


Fig. 5. Comparison of normalized channel gain versus the number of RIS elements N for the different RIS architectures.

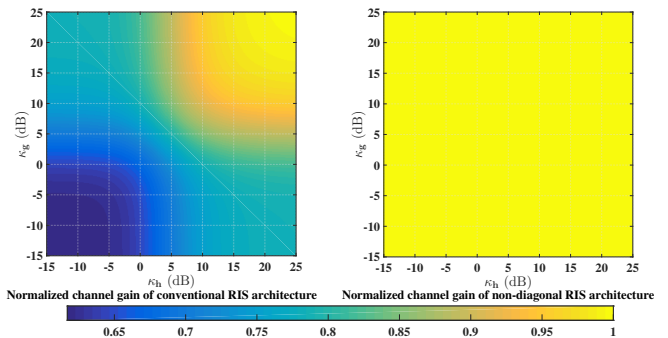


Fig. 6. Comparison of normalized channel gain versus BS-RIS Rician factors $\kappa_{\mathbf{g}}$ and RIS-user Rician factors $\kappa_{\mathbf{h}}$ for the conventional RIS architecture and our proposed RIS architectures.

reflecting elements N . However, regardless of the number of RIS elements N , our RIS architecture outperforms the conventional RIS architecture. This gain is due to the fact that in our RIS architecture, the BS-RIS channel vector \mathbf{g} and the RIS-user channel vector \mathbf{h}^H are combined based on the MRC criterion, when the number of elements N is large.

C. Channel Gain Analysis when $N \rightarrow \infty$

In the conventional RIS architecture, when $N \rightarrow \infty$, according to (56), we can get the average channel gain as

$$\mathfrak{g}_{\text{diag}} = \frac{\pi^2}{16} \varrho_t \varrho_r N^2 \frac{L_{\frac{1}{2}}^2(-\kappa_{\mathbf{g}}) L_{\frac{1}{2}}^2(-\kappa_{\mathbf{h}})}{(\kappa_{\mathbf{g}} + 1)(\kappa_{\mathbf{h}} + 1)}. \quad (78)$$

In our proposed RIS architecture, when $N \rightarrow \infty$, the average channel gain is given by

$$\mathfrak{g}_{\text{nonnd}} = \varrho_t \varrho_r N^2, \quad (79)$$

which is equivalent to the channel gain performance of the fully-connected RIS architecture of [24].

Proof: See Appendix C. ■

Fig. 6 compares the normalized channel gain versus BS-RIS Rician factors $\kappa_{\mathbf{g}}$ and RIS-user Rician factors $\kappa_{\mathbf{h}}$ for the conventional RIS architecture and our proposed RIS architectures. It shows that when $N \rightarrow \infty$, the normalized channel gain of the conventional RIS architecture degrades with the decrease of the Rician factors, while that of our proposed RIS architecture remains at 1 in all Rician factor ranges, which means that our proposed RIS architecture is more robust over a wider range of propagation conditions and especially shows advantages in NLoS-dominated channel environments.

D. Outage Probability and BER Performance Analysis

Since the above analysis demonstrates that our proposed RIS architecture shows advantages in NLoS-dominated chan-

nel environments, in this section we derive the distribution of the received SNR of our proposed RIS architecture in Rayleigh fading channels, then the outage probability and BER performance are analyzed.

According to (88), we can show that the upper bound of the instantaneous SNR at the receiver side of our proposed RIS architecture can be expressed as

$$\Omega = \rho \left(\sum_{i=1}^N a_i^2 \right) \left(\sum_{i=1}^N b_i^2 \right), \quad (80)$$

where we have $\rho = \frac{P_t}{\sigma_n^2} \varrho_t \varrho_r$. Since a_i^2 and b_i^2 both obey the exponential distribution having the rate parameter of $\lambda = 1$, then both $Y_a = \sum_{i=1}^N a_i^2$ and $Y_b = \sum_{i=1}^N b_i^2$ follow the gamma distribution associated with the shape parameter N and the scale parameter 1. Let us introduce $Z = Y_a Y_b$, with the following PDF [43]

$$f_Z(z) = \frac{2}{\Gamma^2(N)} z^{N-1} K_0(2\sqrt{z}), \quad (81)$$

where $\Gamma(\cdot)$ is the gamma function, and $K_0(\cdot)$ is the modified Bessel function of the second kind. Therefore, the CDF of the received SNR Ω is given by

$$F_\Omega(\omega) = \int_0^{\frac{\omega}{\rho}} \frac{2}{\Gamma^2(N)} t^{N-1} K_0(2\sqrt{t}) dt. \quad (82)$$

1) *Outage probability*: If the SNR threshold is ω_{th} , then the outage probability, denoted as $P_{\text{out}}(\omega_{\text{th}})$, can be calculated as [40]

$$P_{\text{out}}(\omega_{\text{th}}) = \Pr(\Omega \leq \omega_{\text{th}}) = \int_0^{\frac{\omega_{\text{th}}}{\rho}} \frac{2}{\Gamma^2(N)} t^{N-1} K_0(2\sqrt{t}) dt. \quad (83)$$

2) *Average BER*: Based on the CDF of the received SNR in (82), the average BER is given by [44]

$$\begin{aligned} P_e &= \frac{q^p}{2\Gamma(p)} \int_0^\infty e^{-q\omega} \omega^{p-1} F_\Omega(\omega) d\omega \\ &= \frac{q^p}{\Gamma(p)\Gamma^2(N)} \int_0^\infty e^{-q\omega} \omega^{p-1} d\omega \int_0^{\frac{\omega}{\rho}} t^{N-1} K_0(2\sqrt{t}) dt, \end{aligned} \quad (84)$$

where the parameters p and q are different for different modulation schemes. For example, we have $p = \frac{1}{2}$ and $q = 1$ for binary phase shift keying (BPSK) modulation [44].

E. Complexity Analysis

In this section, we analyze the complexity of the RIS architecture in terms of the number of configurable impedances required and the BS-RIS control link load.

Firstly, the conventional RIS architecture requires N configurable impedances, while for the fully-connected RIS architecture we need $\frac{N(N+1)}{2}$ and for the group-connected RIS architecture we need $\frac{N(G+1)}{2}$. By contrast, our architecture only requires N configurable impedances, which is the same as that in the conventional RIS architecture. Fig. 7 (a) compares the number of configurable impedances required for the conventional RIS structure, the fully-connected/group-connected RIS structure and our RIS structure, which shows that the number of configurable impedances required by our proposed RIS architecture is lower than that of the fully-connected RIS architecture and of the group-connected RIS architecture.

Secondly, in terms of the BS-RIS control link load, the number of information values transmitted on the BS-RIS control link is N for the conventional RIS architecture, since only the diagonal values of the phase shift matrix are optimized, while for the fully-connected RIS architecture it is $\frac{N(N+1)}{2}$ and for the group-connected RIS architecture it is $\frac{N(G+1)}{2}$. In our proposed non-diagonal phase shift matrix scheme, the number of information values transmitted in BS-RIS control link is $2N$, i.e., N optimized non-zeros values and their positions in the non-diagonal phase shift matrix. Fig. 7 (b) compares the BS-RIS control link load for the conventional RIS structure, the fully-connected/group-connected RIS structure and our RIS structure, which shows that the BS-RIS control link load of our RIS architecture is lower than that of the fully-connected and of the group-connected RIS architecture for $G \geq 4$. However, it has been presented in Fig. 5 that the performance of our proposed RIS structure is better than that of the group-connected method and approaches that of the fully-connected RIS structure, as the number of RIS elements increases.

V. PERFORMANCE RESULTS AND ANALYSIS

In this section, firstly the outage probability and average BER of our proposed RIS architecture are presented. Then, we characterize the achievable rate of our proposed RIS architecture having non-diagonal phase shift matrices.

In Fig. 8 (a), we show the theoretical lower bound of the outage probability of our proposed RIS architecture in (83) versus the number of RIS elements, where the SNR threshold ω_{th} is set to 25dB. Furthermore, the simulation results of our proposed RIS architecture and of the conventional RIS architecture are presented. Note that the theoretical lower bound is very tight, and the performance of our proposed RIS architecture is significantly better than that of the conventional RIS architecture for all values of N . Then, in Fig. 8 (b) we show that our simulation results and the theoretical average BER of our proposed RIS architecture based on (84) match well. The results are contrasted to those using the conventional RIS architecture and to those of the LoS channel, where BPSK modulation is employed. Observe that the average BER performance of our proposed RIS architecture is better than that of the conventional RIS architecture, and tends to that of the LoS channels upon increasing the number of RIS elements.

In the following simulation, the number of antennas at the BS is $M = 4$, the BS-RIS distance d_t is fixed as $d_t = 50\text{m}$, the path loss at the reference distance 1 meter is $C_0 = -30\text{dB}$, the total transmit power is $P_t = 50\text{mW}$, and the noise power is $\sigma_n^2 = -90\text{dBm}$. The Rician factors are $\kappa_G = \kappa_{h_1} = \kappa_{h_2} = \dots = \kappa_{h_K} = -10\text{dB}$, unless otherwise specified.

Firstly, the achievable rate of single-user MISO systems is presented based on (37) in Fig. 9 (a), where we compare the achievable rate versus RIS-user distance d_r of both the conventional RIS and of our proposed RIS structure. The path loss exponent is $\alpha_t = \alpha_r = 2.2$. Observe that the achievable rate decreases upon the increasing the RIS-user distance due to the increased path loss. We can also find that the achievable rate of our proposed RIS architecture is

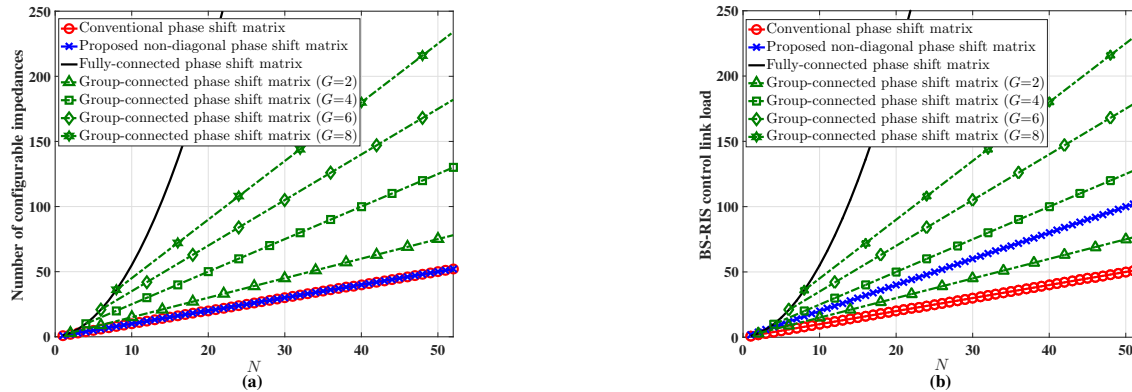


Fig. 7. (a) Comparison of the number of configurable impedances versus the number of RIS elements N for the different RIS architectures. (b) Comparison of the BS-RIS control link load versus the number of RIS elements N for the different RIS architectures.

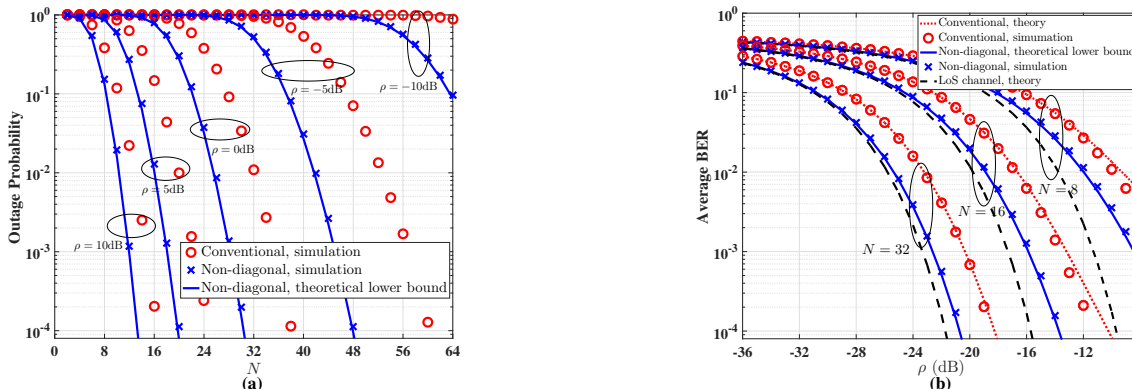


Fig. 8. (a) Theoretical lower bound and simulation results of outage probability versus the number of RIS elements N in conventional RIS structure and our proposed RIS structure. (b) Theoretical analysis and simulation results of average BER versus ρ of conventional RIS architecture, our proposed RIS architecture and LoS channel.

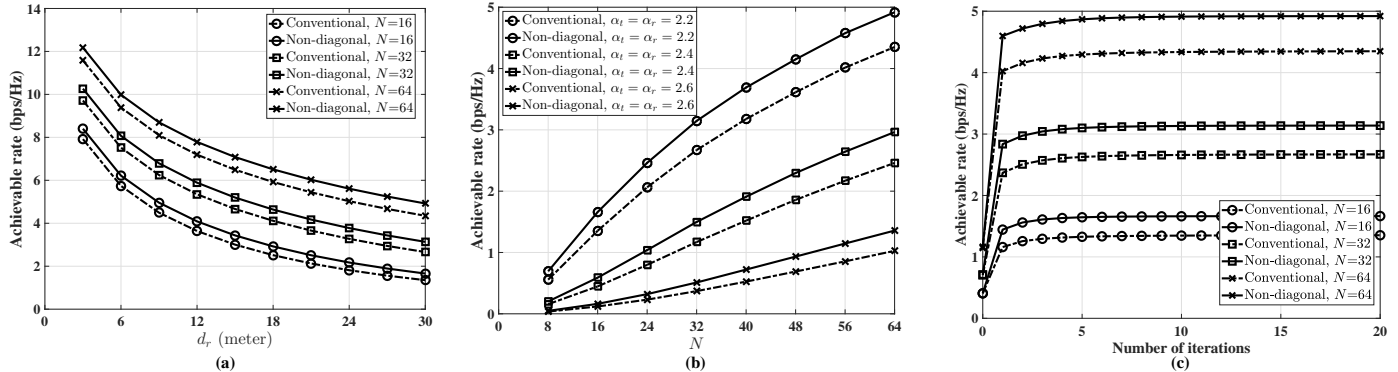


Fig. 9. Comparison of the achievable rate in conventional RIS architecture and our proposed RIS architecture in single-user MISO systems: (a) achievable rate versus RIS-user distance d_r , (b) achievable rate versus the number of RIS elements N , and (c) achievable rate versus the number of iterations in alternating optimization method.

higher than that of the conventional RIS architecture for all RIS-user distances. In Fig. 9 (b), we compare the achievable rate versus the number of RIS elements N in the conventional RIS architecture and our proposed RIS architecture, where the RIS-user distance is $d_r = 30\text{m}$. Observe that the performance of our proposed RIS architecture is better than that of the conventional RIS architecture, especially when the number of RIS elements N is large. This is due to the fact that our proposed RIS architecture benefits from using the MRC criterion upon increasing the number of RIS elements. In Fig. 9 (c), the achievable rate versus the number of iterations in alternating optimization algorithm is presented, where the path loss exponent $\alpha_t = \alpha_r = 2.2$ and RIS-user distance is $d_r = 30\text{m}$. It shows that the convergence speed in our proposed RIS architecture is almost the same as that of the

conventional RIS architecture.

Then, the simulation based on achievable rate of the multi-user MIMO systems is presented in Fig. 10, where the users are distributed uniformly within a half circle centered at the RIS with radius R_D . Explicitly, we compare the achievable rate versus the number of RIS elements N of the conventional and of our proposed RIS architecture. In Fig. 10 (a), the path loss exponent is $\alpha_t = \alpha_r = 2.2$, and the number of users is $K = 2$. It can be seen that compared to the conventional RIS architecture, our proposed RIS architecture has better coverage under the same data rate requirement. In Fig. 10 (b), the path loss exponent is $\alpha_t = \alpha_r = 2.2$, and the radius is $R_D = 30\text{m}$, where it can be seen that the achievable rate increases near linearly with the number of RIS elements. Compared to the conventional RIS architecture, the achievable rate of our

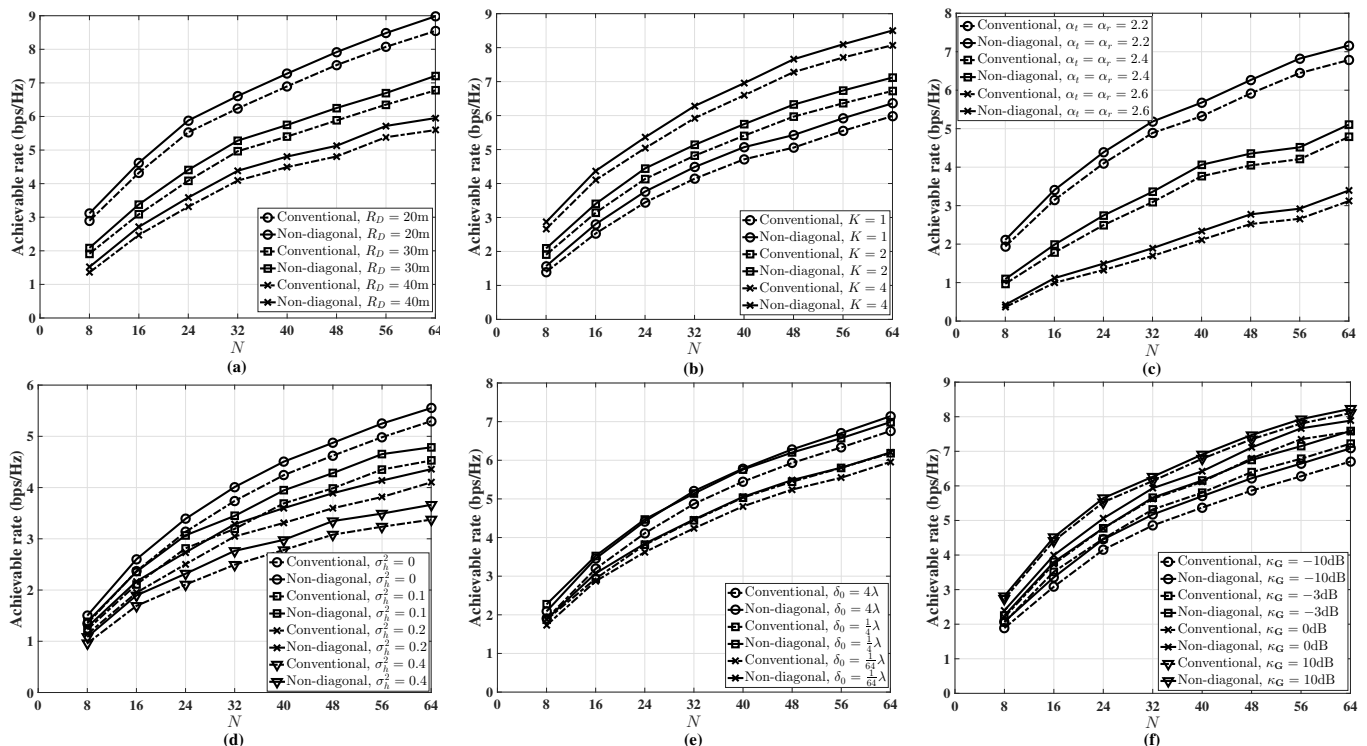


Fig. 10. Comparison of the achievable rate versus the number of RIS elements N in conventional RIS structure and our proposed RIS structure in multi-user MIMO systems: (a) with the user radius $R_D = 20\text{m}, 30\text{m}, 40\text{m}$, (b) with the number of users $K = 1, 2, 4$, (c) with the path loss exponent $\alpha = 2.2, 2.4, 2.6$, (d) with channel estimation error variance $\sigma_h^2 = 0, 0.1, 0.2, 0.4$, (e) with the distance between adjacent RIS elements $\delta_0 = 4\lambda, \frac{1}{4}\lambda, \frac{1}{64}\lambda$, and (f) with Rician factor $\kappa_G = -10\text{dB}, -3\text{dB}, 0\text{dB}, 10\text{dB}$.

proposed method is significantly high for any number of users. In Fig. 10 (c), the number of users is $K = 2$, and the radius is $R_D = 30\text{m}$. We can observe the performance enhancement of our proposed RIS architecture when the number of RIS elements N is large for any pathloss exponent value.

When considering imperfect CSI, referring to [45], the estimated BS-RIS and RIS-user channels are given by $\hat{\mathbf{g}}_m = \mathbf{g}_m + \mathbf{g}_{m,e}$ and $\hat{\mathbf{h}}_k^H = \mathbf{h}_k^H + \mathbf{h}_{k,e}^H$, respectively, where $m = 1, 2, \dots, M$, $k = 1, 2, \dots, K$. The channel estimation error component obeys $\mathbf{g}_{m,e} \sim \mathcal{CN}(\mathbf{0}, \sigma_h^2 \mathbf{I})$, $\mathbf{h}_{k,e}^H \sim \mathcal{CN}(\mathbf{0}, \sigma_h^2 \mathbf{I})$, where σ_h^2 represents the estimation error variance. In the linear minimum mean squared error (LMMSE) method, we have $\sigma_h^2 = \frac{1}{1 + \tau_p \rho_t}$, where ρ_t is the pilot transmission power and τ_p represents the pilot symbols transmission duration [46]. In Fig. 10 (d), the achievable rate is presented when considering imperfect CSI, where the path loss exponent is $\alpha_t = \alpha_r = 2.2$, the number of users is $K = 2$ and the radius is $R_D = 30\text{m}$. As shown in Fig. 10 (d), our proposed RIS architecture outperforms the conventional RIS architecture under any channel estimation error variance σ_h^2 , which shows the robustness of our proposed architecture compared to the conventional one.

In most of the previous contributions [12]–[15], [17]–[24], it is assumed that the distance between the adjacent RIS elements is large enough to ensure that the BS-RIS and RIS-user channels are uncorrelated. To make our work more realistic, in Fig. 10 (e), we employ the exponential correlation channel model of [47] to investigate the effect of channel correlation on the achievable rate, where the path loss exponent is $\alpha_t = \alpha_r = 2.2$, the number of users is $K = 2$, the radius is $R_D = 30\text{m}$ and the reference correlation

distance $d_{\text{ref}} = \lambda$. As shown in Fig. 10 (e), our proposed RIS architecture attains a better performance than that of the conventional RIS architecture. For example, the achievable rate in our proposed RIS architecture with adjacent RIS element distance $\delta_0 = \frac{1}{64}\lambda$ is almost the same as that in conventional RIS architecture with adjacent RIS element distance $\delta_0 = \frac{1}{4}\lambda$, and the achievable rate in our proposed RIS architecture with adjacent RIS element distance $\delta_0 = \frac{1}{4}\lambda$ is even higher than that in conventional RIS architecture with adjacent RIS element distance $\delta_0 = 4\lambda$.

Finally, we investigate the impact of the Rician factor on the achievable rate in Fig. 10 (f), where the path loss exponent is $\alpha_t = \alpha_r = 2.2$, the number of users is $K = 2$, the radius is $R_D = 30\text{m}$. We also assume the Rician factor of RIS-user path is $\kappa_{h_r} = -20\text{dB}$ for $k = 1, 2, \dots, K$, while the Rician factor of BS-RIS path κ_G can range between -10dB to 10dB . With the increase of the Rician factor κ_G , the achievable rate of the conventional RIS architecture and that of our proposed RIS architecture can both achieve better performance, which is due to the reduced impact of channel fading with the increase of LoS component. Besides, it shows that the achievable rate enhancement of our proposed RIS architecture is not obvious in the high range of Rician factor, while it is significant when the channel is dominated by NLoS component, which agrees with the above theoretical analysis.

VI. CONCLUSIONS

In this paper, we proposed a novel RIS architecture, where the signal impinging on a specific element can be reflected by another element after phase shift adjustment. Compared to the conventional RIS architecture, our proposed RIS architecture

provides better channel gain as a benefit of using the MRC criterion. The theoretical analysis showed that our system performs better than the conventional RIS system both in terms of its average channel gain, outage probability and average BER. Furthermore, the performance of our proposed RIS architecture is better than that of the group-connected RIS architecture and approaches that of the fully-connected RIS architecture, with increasing the number of RIS elements, despite its considerably reduced complexity compared to the fully-connected architecture. Furthermore, we formulated and solved the problem of maximizing the achievable rate of our proposed RIS architecture by jointly optimizing the active TBF and the non-diagonal phase shift matrix of both single-user MISO systems and of multi-user MIMO systems based on alternating optimization and on SDR methods, respectively. The simulation results showed that our proposed technique is capacity of enhancing the achievable rate of RIS-assisted wireless communications.

APPENDIX A PROOF OF FORMULA (65)

When $\kappa_g \rightarrow \infty$, according to (46), we can get that $a_i = 1$ ($i = 1, 2, \dots, N$). Therefore,

$$\sum_{i=1}^N a_i b_i = \sum_{i=1}^N a_{(i)} b_{(i)} = \sum_{i=1}^N b_i. \quad (85)$$

According to (55), (57) and (85), we can show that $\mathfrak{g}_{\text{diag}} = \mathfrak{g}_{\text{nonnd}}$. When we consider the case that $\kappa_h \rightarrow \infty$, we can similarly get that $\mathfrak{g}_{\text{diag}} = \mathfrak{g}_{\text{nonnd}}$. The proof is thus completed.

APPENDIX B PROOF OF *Theorem 1*

We denote the CDF of the random variable X following the Rayleigh distribution with the scale parameter σ as $F_X(x; \sigma)$. The PDF of $a_{(i)}$ is given by [42]

$$\begin{aligned} f_{a_{(i)}}(x) &= C_{i,N} f_X \left(x; \sigma = \frac{\sqrt{2}}{2} \right) \left[F_X \left(x; \sigma = \frac{\sqrt{2}}{2} \right) \right]^{i-1} \times \\ &\quad \left[1 - F_X \left(x; \sigma = \frac{\sqrt{2}}{2} \right) \right]^{N-i} \\ &= 2C_{i,N} x e^{-x^2} \left(1 - e^{-x^2} \right)^{i-1} \left(e^{-x^2} \right)^{N-i} \\ &= 2C_{i,N} x \left(1 - e^{-x^2} \right)^{i-1} \left(e^{-x^2} \right)^{N-(i-1)}. \end{aligned} \quad (86)$$

In (86), $\left(1 - e^{-x^2} \right)^{i-1} = \sum_{k=0}^{i-1} \binom{i-1}{k} \left(-e^{-x^2} \right)^k$, so

$$\begin{aligned} f_{a_{(i)}}(x) &= 2C_{i,N} x \left(e^{-x^2} \right)^{N-(i-1)} \sum_{k=0}^{i-1} \binom{i-1}{k} \left(-e^{-x^2} \right)^k \\ &= 2C_{i,N} \sum_{k=0}^{i-1} \binom{i-1}{k} x \left(-e^{-x^2} \right)^{N-(i-1)+k} \\ &= C_{i,N} \sum_{k=0}^{i-1} \binom{i-1}{k} \frac{1}{N-i+k+1} (-1)^k \times \\ &\quad f_X \left(x; \sigma = \frac{1}{\sqrt{2(N-i+k+1)}} \right) \end{aligned}$$

$$\begin{aligned} &= \sum_{k=0}^{i-1} \binom{N}{i-k-1} \binom{N-i+k}{k} (-1)^k \times \\ &\quad f_X \left(x; \sigma = \frac{1}{\sqrt{2(N-i+k+1)}} \right). \end{aligned} \quad (87)$$

The proof is thus completed.

APPENDIX C PROOF OF FORMULA (79)

In (57), according to Cauchy-Schwarz inequality, we can get

$$\begin{aligned} \mathfrak{g}_{\text{nonnd}} &= \varrho_t \varrho_r \mathbb{E} \left(\left(\sum_{i=1}^N a_{(i)} b_{(i)} \right)^2 \right) \\ &\leq \varrho_t \varrho_r \mathbb{E} \left(\left(\sum_{i=1}^N a_{(i)}^2 \right) \left(\sum_{i=1}^N b_{(i)}^2 \right) \right), \end{aligned} \quad (88)$$

where the equality in (88) is established only when $a_{(i)} = b_{(i)}$. When $N \rightarrow \infty$, we can get

$$a_{(i)} = b_{(i)} = F_{a_i}^{-1} \left(\frac{i}{N} \right) = F_{b_i}^{-1} \left(\frac{i}{N} \right), \quad (89)$$

where $F_{a_i}^{-1}(\cdot)$ and $F_{b_i}^{-1}(\cdot)$ represent the inverse CDF of $a_{(i)}$ and $b_{(i)}$, respectively. Based on (88) and (89), we can show that when $N \rightarrow \infty$, the channel gain of our proposed RIS architecture is

$$\begin{aligned} \mathfrak{g}_{\text{nonnd}} &= \varrho_t \varrho_r \mathbb{E} \left(\left(\sum_{i=1}^N a_{(i)}^2 \right) \left(\sum_{i=1}^N b_{(i)}^2 \right) \right) \\ &= \varrho_t \varrho_r \mathbb{E} \left(\sum_{i=1}^N a_i^2 \right) \mathbb{E} \left(\sum_{i=1}^N b_i^2 \right) \\ &= \varrho_t \varrho_r N^2. \end{aligned} \quad (90)$$

The proof is thus completed.

REFERENCES

- [1] Z. Ma, M. Xiao, Y. Xiao, Z. Pang, H. V. Poor, and B. Vucetic, "High-reliability and low-latency wireless communication for Internet of Things: challenges, fundamentals, and enabling technologies," *IEEE Internet of Things Journal*, vol. 6, no. 5, pp. 7946–7970, 2019.
- [2] H. Yetgin, K. T. K. Cheung, M. El-Hajjar, and L. H. Hanzo, "A survey of network lifetime maximization techniques in wireless sensor networks," *IEEE Communications Surveys & Tutorials*, vol. 19, no. 2, pp. 828–854, 2017.
- [3] F. Boccardi, R. W. Heath, A. Lozano, T. L. Marzetta, and P. Popovski, "Five disruptive technology directions for 5G," *IEEE communications magazine*, vol. 52, no. 2, pp. 74–80, 2014.
- [4] M. A. ElMossallamy, H. Zhang, L. Song, K. G. Seddik, Z. Han, and G. Y. Li, "Reconfigurable intelligent surfaces for wireless communications: Principles, challenges, and opportunities," *IEEE Transactions on Cognitive Communications and Networking*, vol. 6, no. 3, pp. 990–1002, 2020.
- [5] M. Di Renzo, A. Zappone, M. Debbah, M.-S. Alouini, C. Yuen, J. de Rosny, and S. Tretyakov, "Smart radio environments empowered by reconfigurable intelligent surfaces: How it works, state of research, and the road ahead," *IEEE Journal on Selected Areas in Communications*, vol. 38, no. 11, pp. 2450–2525, 2020.
- [6] S. Gong, X. Lu, D. T. Hoang, D. Niyato, L. Shu, D. I. Kim, and Y.-C. Liang, "Toward smart wireless communications via intelligent reflecting surfaces: A contemporary survey," *IEEE Communications Surveys & Tutorials*, vol. 22, no. 4, pp. 2283–2314, 2020.
- [7] C. Pan, H. Ren, K. Wang, W. Xu, M. ElKashlan, A. Nallanathan, and L. Hanzo, "Multicell MIMO communications relying on intelligent reflecting surfaces," *IEEE Transactions on Wireless Communications*, vol. 19, no. 8, pp. 5218–5233, 2020.

- [8] L. Dai, B. Wang, M. Wang, X. Yang, J. Tan, S. Bi, S. Xu, F. Yang, Z. Chen, M. Di Renzo, C.-B. Chae, and L. Hanzo, "Reconfigurable intelligent surface-based wireless communications: Antenna design, prototyping, and experimental results," *IEEE Access*, vol. 8, pp. 45 913–45 923, 2020.
- [9] T. Hou, Y. Liu, Z. Song, X. Sun, Y. Chen, and L. Hanzo, "Reconfigurable intelligent surface aided NOMA networks," *IEEE Journal on Selected Areas in Communications*, vol. 38, no. 11, pp. 2575–2588, 2020.
- [10] Z. Zhou, N. Ge, Z. Wang, and L. Hanzo, "Joint transmit precoding and reconfigurable intelligent surface phase adjustment: A decomposition-aided channel estimation approach," *IEEE Transactions on Communications*, vol. 69, no. 2, pp. 1228–1243, 2020.
- [11] X. Cao, B. Yang, C. Huang, C. Yuen, M. Di Renzo, Z. Han, D. Niyato, H. V. Poor, and L. Hanzo, "AI-assisted MAC for reconfigurable intelligent surface-aided wireless networks: Challenges and opportunities," *IEEE Communications Magazine*, vol. 59, no. 6, pp. 21–27, 2021.
- [12] Q. Wu and R. Zhang, "Intelligent reflecting surface enhanced wireless network via joint active and passive beamforming," *IEEE Transactions on Wireless Communications*, vol. 18, no. 11, pp. 5394–5409, 2019.
- [13] B. Ning, Z. Chen, W. Chen, and J. Fang, "Beamforming optimization for intelligent reflecting surface assisted MIMO: A sum-path-gain maximization approach," *IEEE Wireless Communications Letters*, vol. 9, no. 7, pp. 1105–1109, 2020.
- [14] P. Wang, J. Fang, X. Yuan, Z. Chen, and H. Li, "Intelligent reflecting surface-assisted millimeter wave communications: Joint active and passive precoding design," *IEEE Transactions on Vehicular Technology*, vol. 69, no. 12, pp. 14 960–14 973, 2020.
- [15] Y. Han, W. Tang, S. Jin, C.-K. Wen, and X. Ma, "Large intelligent surface-assisted wireless communication exploiting statistical CSI," *IEEE Transactions on Vehicular Technology*, vol. 68, no. 8, pp. 8238–8242, 2019.
- [16] J. Wang, H. Wang, Y. Han, S. Jin, and X. Li, "Joint transmit beamforming and phase shift design for reconfigurable intelligent surface assisted MIMO systems," *IEEE Transactions on Cognitive Communications and Networking*, vol. 7, no. 2, pp. 354–368, 2021.
- [17] Q. Wu and R. Zhang, "Beamforming optimization for wireless network aided by intelligent reflecting surface with discrete phase shifts," *IEEE Transactions on Communications*, vol. 68, no. 3, pp. 1838–1851, 2019.
- [18] S. Zhang, H. Zhang, B. Di, Y. Tan, Z. Han, and L. Song, "Beyond intelligent reflecting surfaces: Reflective-transmissive metasurface aided communications for full-dimensional coverage extension," *IEEE Transactions on Vehicular Technology*, vol. 69, no. 11, pp. 13 905–13 909, 2020.
- [19] W. Chen, X. Ma, Z. Li, and N. Kuang, "Sum-rate maximization for intelligent reflecting surface based Terahertz communication systems," in *2019 IEEE/CIC International Conference on Communications Workshops in China (ICCC Workshops)*. IEEE, 2019, pp. 153–157.
- [20] J. Xu, W. Xu, and A. L. Swindlehurst, "Discrete phase shift design for practical large intelligent surface communication," in *2019 IEEE Pacific Rim Conference on Communications, Computers and Signal Processing (PACRIM)*. IEEE, 2019, pp. 1–5.
- [21] S. Lin, B. Zheng, G. C. Alexandropoulos, M. Wen, M. Di Renzo, and F. Chen, "Reconfigurable intelligent surfaces with reflection pattern modulation: Beamforming design and performance analysis," *IEEE Transactions on Wireless Communications*, vol. 20, no. 2, pp. 741–754, 2020.
- [22] E. Basar, M. Di Renzo, J. De Rosny, M. Debbah, M.-S. Alouini, and R. Zhang, "Wireless communications through reconfigurable intelligent surfaces," *IEEE Access*, vol. 7, pp. 116 753–116 773, 2019.
- [23] L. Yang, F. Meng, Q. Wu, D. B. da Costa, and M.-S. Alouini, "Accurate closed-form approximations to channel distributions of RIS-aided wireless systems," *IEEE Wireless Communications Letters*, vol. 9, no. 11, pp. 1985–1989, 2020.
- [24] S. Shen, B. Clerckx, and R. Murch, "Modeling and architecture design
- [27] S. Abeywickrama, R. Zhang, Q. Wu, and C. Yuen, "Intelligent reflecting surface: Practical phase shift model and beamforming optimization," *IEEE Transactions on Communications*, vol. 68, no. 9, pp. 5849–5863, 2020.
- of intelligent reflecting surfaces using scattering parameter network analysis," *IEEE Transactions on Wireless Communications*, 2021.
- [25] Q. Wu, S. Zhang, B. Zheng, C. You, and R. Zhang, "Intelligent reflecting surface aided wireless communications: A tutorial," *IEEE Transactions on Communications*, 2021.
- [26] A. Wang, R. Yin, and C. Zhong, "Channel estimation for uniform rectangular array based massive MIMO systems with low complexity," *IEEE Transactions on Vehicular Technology*, vol. 68, no. 3, pp. 2545–2556, 2019.
- [28] Y. Liu, X. Liu, X. Mu, T. Hou, J. Xu, M. Di Renzo, and N. Al-Dhahir, "Reconfigurable intelligent surfaces: Principles and opportunities," *IEEE Communications Surveys & Tutorials*, 2021.
- [29] G. M. Rebeiz and J. B. Muldavin, "RF MEMS switches and switch circuits," *IEEE Microwave magazine*, vol. 2, no. 4, pp. 59–71, 2001.
- [30] V. Laur, J. Gouavogui, and B. Balde, "C-band hybrid 3-D-printed microwave isolator," *IEEE Transactions on Microwave Theory and Techniques*, vol. 69, no. 3, pp. 1579–1585, 2021.
- [31] S. Yang, D. Vincent, J. R. Bray, and L. Roy, "Study of a ferrite LTCC multifunctional circulator with integrated winding," *IEEE Transactions on Components, Packaging and Manufacturing Technology*, vol. 5, no. 7, pp. 879–886, 2015.
- [32] J. Wang, A. Yang, Y. Chen, Z. Chen, A. Geiler, S. M. Gillette, V. G. Harris, and C. Vittoria, "Self-biased Y-junction circulator at K_u band," *IEEE Microwave and Wireless Components Letters*, vol. 21, no. 6, pp. 292–294, 2011.
- [33] W. D'orazio, K. Wu, and J. Helszajn, "A substrate integrated waveguide degree-2 circulator," *IEEE Microwave and Wireless Components Letters*, vol. 14, no. 5, pp. 207–209, 2004.
- [34] S. Adhikari, A. Ghiotto, S. Hemour, and K. Wu, "Tunable non-reciprocal ferrite loaded SIW phase shifter," in *2013 IEEE MTT-S International Microwave Symposium Digest (MTT)*. IEEE, 2013, pp. 1–3.
- [35] A. Li, S. Singh, and D. Sievenpiper, "Metasurfaces and their applications," *Nanophotonics*, vol. 7, no. 6, pp. 989–1011, 2018.
- [36] C. Liaskos, G. G. Pyrialakos, A. Pitolakis, A. Tsioliaridou, M. Christodoulou, N. Kantartzis, S. Ioannidis, A. Pitsillides, and I. F. Akyildiz, "The internet of metamaterial things and their software enablers," *ITU Journal on Future and Evolving Technologies*, 2020.
- [37] S. Boyd, S. P. Boyd, and L. Vandenberghe, *Convex optimization*. Cambridge university press, 2004.
- [38] X.-D. Zhang, *Matrix analysis and applications*. Cambridge University Press, 2017.
- [39] M. Grant, S. Boyd, and Y. Ye, "CVX: Matlab software for disciplined convex programming," 2008.
- [40] D. Tse and P. Viswanath, *Fundamentals of wireless communication*. Cambridge university press, 2005.
- [41] A. Abdi, C. Tepedelenlioglu, M. Kaveh, and G. Giannakis, "On the estimation of the K parameter for the rice fading distribution," *IEEE Communications letters*, vol. 5, no. 3, pp. 92–94, 2001.
- [42] A. Rényi, "On the theory of order statistics," *Acta Mathematica Academiae Scientiarum Hungarica*, vol. 4, no. 3-4, pp. 191–231, 1953.
- [43] C. S. Withers and S. Nadarajah, "On the product of gamma random variables," *Quality & Quantity*, vol. 47, no. 1, pp. 545–552, 2013.
- [44] I. S. Ansari, S. Al-Ahmadi, F. Yilmaz, M.-S. Alouini, and H. Yanikomeroglu, "A new formula for the BER of binary modulations with dual-branch selection over generalized-K composite fading channels," *IEEE Transactions on Communications*, vol. 59, no. 10, pp. 2654–2658, 2011.
- [45] T. Yoo and A. Goldsmith, "Capacity of fading MIMO channels with channel estimation error," in *2004 IEEE International Conference on Communications (IEEE Cat. No. 04CH37577)*, vol. 2. IEEE, 2004, pp. 808–813.
- [46] S. Katla, L. Xiang, Y. Zhang, M. El-Hajjar, A. A. Mourad, and L. Hanzo, "Deep learning assisted detection for index modulation aided mmwave systems," *IEEE Access*, vol. 8, pp. 202 738–202 754, 2020.
- [47] J. R. Hampton, *Introduction to MIMO communications*. Cambridge university press, 2013.